Supporting Information for

Addition of a Second Binding Site Increases the Dynamic Range but Alters the Cellular Localization of a Red Fluorescent Probe for Mobile Zinc

Andrei Loas, Robert J. Radford, and Stephen J. Lippard*

TABLE OF CONTENTS

Experimental Section

General Methods. Syntheses involving air-sensitive compounds were performed using a five-port double-manifold Schlenk line. Inert gas atmosphere was provided by a zero-grade, in-house nitrogen line. Reaction mixtures were monitored by thin-layer chromatography (TLC) on pre-coated, aluminum-backed silica gel 60 F_{254} plates. Gel filtration and flash chromatography were performed on silica gel 60 (230-400 mesh). HPLC separations were carried out at the semi-preparative scale on an Agilent 1200 Series system equipped with multi-wavelength detector and automated fraction collector, using a reverse stationary phase column (Zorbax SB-C18, 5 μm, 9.5 mm × 250 mm). Analytical HPLC was performed on a similar system using a Zorbax SB-C18 reverse stationary phase column (5 μm, 4.6 mm × 250 mm). FT-NMR spectra were acquired at ambient temperature on a Bruker Avance III 400 or a Varian Inova 500 instrument. ^{13}C NMR spectra were acquired with proton decoupling. Assignment of all chemical shifts is based on the 1D spectral data. ^{1}H and ^{13}C chemical shifts are reported in ppm relative to $SiMe_4$ ($\delta = 0.00$) and were referenced internally to the residual solvent signals.[1] Low-resolution mass spectra (MS) were acquired on an Agilent 1100 Series LC/MSD Trap spectrometer by electrospray ionization (ESI). The MIT Department of Chemistry Instrumentation Facility acquired high-resolution mass spectra (HRMS) using the ESI technique on a Bruker Daltonics APEXIV 4.7 T FT-ICR-MS instrument. Electronic absorption spectra were collected in absorbance mode on a Varian Cary 50 Bio UV-vis spectrophotometer. Fluorescence spectra were acquired on a Quanta Master 4 L-format scanning spectrofluorimeter (Photon Technology International). The samples for UV-visible and fluorescence spectroscopy were prepared as dilute (1-20 μM) solutions of the analyte in 1.0 cm quartz cuvettes. Infrared spectra were obtained as an average of 32 scans using an Avatar 360 FT-IR spectrophotometer (Thermo Nicolet) with a resolution of 2 cm^{-1}. The samples for infrared spectroscopy were prepared by grinding the analyte with KBr to a fine powder and pressing into pellets. Melting points were obtained in triplicate using capillary tubes in air with an OptiMelt automated instrument (Stanford Research Systems) and are uncorrected.

Materials. All solvents employed were ACS reagent grade or higher. Acetonitrile was kept dry under activated 3 Å molecular sieves; 2,2'-dipicolylamine (DPA) was freshly distilled before use. All other solvents and reagents were purchased from commercial sources and used as received.

Synthesis of 4-Chloro-6-nitrosoresorcinol (2). 4-Chlororesorcinol (**1**, 14.6 g, 0.1 mol) was dissolved in a solution of KOH (7.4 g, 0.132 mol) in 20 mL of water and 80 mL of EtOH. To this dark brown solution, isoamyl nitrite (12.2 g, 16.0 mL, 0.104 mol) was added dropwise with stirring at 0-5 °C over 30 min. The mixture was allowed to warm to room temperature and stirring was continued for an additional 1 h. The solution was brought to pH ~2 by addition of conc. aq. HCl. A yellow precipitate formed, which was filtered, washed with 50 mL of cold water and dried under air suction overnight to afford pure **2** as a yellow powder in 84% yield (14.52 g). Mp: 125-128 °C; IR (KBr): 3281, 3072, 1612, 1566, 1440, 1327, 1215, 1056, 998, 852 cm^{-1}; ^{1}H NMR (400 MHz, $(CD_3)_2SO$): δ 13.86 (br, 1H, Ar-O*H*), 11.41 (br, 1H, Ar-O*H*), 7.67 (s, 1H, Ar-*H*), 5.81 (s, 1H, Ar-*H*); ^{13}C {^{1}H} NMR (100 MHz, $(CD_3)_2SO$): δ 178.8, 162.5, 144.3, 135.7, 119.5, 105.6; MS (ESI−): *m/z* calcd for $[M - H]^-$ $(C_6H_3O_3NCl)^-$ 172.0, found 171.8.

Synthesis of 10-Chloro-9-hydroxy-5*H*-benzo[*a*]phenoxazin-5-one (3). 1,3-Dihydroxy-naphthalene (1.61 g, 10.0 mmol) was dissolved in 10 mL of conc. H_2SO_4 and heated to 85 °C with stirring. After 10 min, solid **2** (1.75 g, 10.1 mmol) was added in portions over 10 min. The mixture was then stirred at 90-95 °C for 20 h, cooled to room temperature and poured with stirring into 300 mL of ice-water. After stirring for 10 min, the suspension was allowed to settle for 30 min at 4 °C. The resulting precipitate was filtered, washed with water (200 mL), and dried under air suction for 3 h, then at 80 °C in vacuo to constant weight to afford chlorobenzoresorufin **3** as a dark violet powder in >99% yield (2.94 g). The product is insoluble in most organic solvents and was used without further purification. Mp: >300 °C; IR (KBr): 3427, 1622, 1587, 1178, 1032, 766, 642, 526 cm^{-1}; ^{1}H NMR (400 MHz, CD_3COOD): δ 8.74 (d, J = 7.9 Hz, 1H, Ar-*H*), 8.32 (d, J = 7.9 Hz, 1H, Ar-*H*), 7.93 (s, 1H, Ar-*H*), 7.83 (m, 2H, Ar-*H*), 7.08 (s, 1H, Ar-*H*), 6.62 (s, 1H, Ar-*H*); MS (ESI+): *m/z* calcd for $[M + H]^+$ $(C_{16}H_9O_3NCl)^+$ 298.0, found 297.9.

Synthesis of 10-Chloro-5-oxo-5*H*-benzo[*a*]phenoxazin-9-yl acetate (4). Chlorobenzo-resorufin **3** (1.8 g, 8.0 mmol) was treated with 25 mL of acetic anhydride and 2 mL of dry pyridine and heated under a nitrogen atmosphere with stirring at reflux for 20 h. The reaction mixture was cooled to room temperature, poured into 300 mL of ice-water, stirred for 10 min and allowed to settle for 30 min at 4 °C. The precipitate was filtered, washed with water (100 mL) and dried under air suction for 3 h to furnish a crude brown solid containing mostly starting

material **3**, which was not completely solubilized under the reaction conditions. This solid was charged to a silica gel column and purified twice by flash chromatography (EtOAc/hexanes = 1:2, then EtOAc/DCM = 0:100 to 5:95), collecting each time the first product fraction as a yellow solid. Triturating this solid with 10 mL of Et_2O/pentane = 1:1 followed by drying in vacuo afforded pure **4** as a bright yellow powder in 5% yield (0.11 g). Mp: 230-232 °C (from DCM); IR (KBr): 2922, 2852, 1776, 1637, 1464, 1173, 1028, 804 cm^{-1}; ^1H NMR (400 MHz, $CDCl_3$): δ 8.66 (m, 1H, Ar-*H*), 8.28 (m, 1H, Ar-*H*), 7.90 (s, 1H, Ar-*H*), 7.77 (m, 2H, Ar-*H*), 7.15 (s, 1H, Ar-*H*), 6.43 (s, 1H, Ar-*H*), 2.41 (s, 3H, Ar-COCH_3); ^{13}C {^1H} NMR (100 MHz, $CDCl_3$): δ 183.7, 167.9, 150.4, 148.4, 148.2, 142.9, 132.3 (overlap), 132.1, 131.3, 130.9, 130.3, 126.1, 124.9, 123.5, 111.4, 108.2, 20.7; MS (ESI+): *m/z* calcd for $[M + H]^+$ $(C_{18}H_{11}O_4NCl)^+$ 340.0, found 340.0.

Synthesis of 6,8-Bis((bis(pyridin-2-ylmethyl)amino)methyl)-10-chloro-9-hydroxy-5*H*-benzo[*a*]phenoxazin-5-one (ZBR4, 5). DPA (0.2 g, 1.0 mmol) and paraformaldehyde (0.03 g, 1.0 mmol) were mixed in 10 mL of dry CH_3CN and heated to reflux for 30 min under nitrogen atmosphere. To this clear solution, a suspension of **4** (0.065 g, 0.19 mmol) in 10 mL of dry CH_3CN and 1 mL of $CHCl_3$ was added dropwise, and the mixture was then heated to reflux under nitrogen atmosphere with stirring for 20 h. After cooling to room temperature, the reaction mixture was diluted with 100 mL of DCM, washed with water (3 × 100 mL) and brine (100 mL), and concentrated under reduced pressure to a dark brown oily solid. The crude product was purified twice by semi-preparative reverse phase HPLC using the (A) water (0.1% v/v TFA) / (B) CH_3CN (0.1% v/v TFA) solvent system, according to the following protocol: constant flow rate 3 mL min^{-1}; 5 min, isocratic flow 10% B; 5 min, linear gradient 10-35% B; 8 min, linear gradient 35-45% B. The equivalent fractions from independent runs were combined and lyophilized to afford the TFA salt of ZBR4 (**5**) as a dark brown powder in 15% yield (18 mg). The purity was judged to be ~98% by analytical HPLC (Figure S16A), employing the solvent system above according to the following protocol: constant flow rate 1 mL min^{-1}; 5 min, isocratic flow 10% B; 30 min, linear gradient 10-50% B; retention time: 26.8 min. IR (KBr): 3429, 2920, 1684, 1632, 1587, 1385, 1201, 1134, 798, 721 cm^{-1}; ^1H NMR (500 MHz, $CDCl_3$): δ 8.75 (d, J = 5.6 Hz, 2H, Py-*H*), 8.69 (d, J = 5.2 Hz, 2H, Py-*H*), 8.59 (d, J = 7.9 Hz, 1H, Ar-*H*), 8.25 (d, J = 7.8 Hz, 1H, Ar-*H*), 8.02 (m, 4H, Py-*H*), 7.94 (d, J = 7.9 Hz, 2H, Py-*H*), 7.77 (s, 1H,

Ar-*H*), 7.75 (m, 3H, 2Py-*H*, 1Ar-*H*), 7.70 (t, *J* = 7.8 Hz, 1H, Ar-*H*), 7.47 (t, *J* = 6.4 Hz, 4H, Py-*H*), 4.65 (s, 4H, Py-CH_2), 4.40 (s, 4H, Py-CH_2), 4.34 (s, 2H, Ar-CH_2), 4.32 (s, 2H, Ar-CH_2); ^{13}C {^{1}H} NMR (125 MHz, $CDCl_3$): 183.25, 158.8, 156.6, 153.1, 149.7, 146.4, 145.6, 141.95, 141.5, 140.2 (overlap), 132.3, 131.1 (overlap), 130.7, 130.0, 125.9, 125.85, 125.1, 124.2 (overlap), 124.1, 123.35, 120.55, 111.1, 109.8, 57.8, 57.35, 48.45, 47.5; ^{19}F NMR (376 MHz, $(CD_3)_2CO$): −76.48 (s, 3F, CF_3COO$^-$); HRMS (ESI+): *m/z* calcd for $[M + H]^+$ $(C_{42}H_{35}O_3N_7Cl)^+$ 720.2490, found 720.2482.

Synthesis of 2,8-Dichloro-7-hydroxy-3*H*-phenoxazin-3-one (6). 4-Chlororesorcinol (**1**, 1.45 g, 10.0 mmol) was dissolved in 10 mL of conc. H_2SO_4 and heated to 85 °C with stirring. The mixture became a homogeneous dark red solution within 10 min, to which **2** (1.74 g, 10.0 mmol) was added in portions over 10 min. The mixture was then heated to 110 °C with stirring for 20 h, cooled to room temperature and poured with stirring into 300 mL of ice-water. After 10 min, the precipitate was filtered, washed with water (2 × 200 mL), and dried under air suction for 3 h, then at 80 °C in vacuo to afford pure dichlororesorufin **6** as a dark brown powder in >99% yield (2.83 g). The product is insoluble in most organic solvents and was used without further purification. Mp: >300 °C; ^{1}H NMR (400 MHz, CD_3COOD): δ 7.90 (s, 2H, Ar-*H*), 6.87 (s, 2H, Ar-*H*); MS (ESI−): *m/z* calcd for $[M - H]^-$ $(C_{12}H_4O_3NCl_2)^-$ 280.0, found 279.8.

Synthesis of 2,8-Dichloro-3-oxo-3*H*-phenoxazin-7-yl acetate (7). Dichlororesorufin **6** (1.41 g, 5.0 mmol) was treated with 10 mL of acetic anhydride and 1 mL of dry pyridine and stirred under nitrogen at room temperature for 40 h. The reaction mixture was poured into 300 mL of ice-water, stirred for 10 min and allowed to settle for 30 min at 4 °C. The precipitate was then filtered, washed with water (100 mL), and dried under air suction for 3 h and finally at 80 °C in vacuo for 3 h to furnish pure **7** as an orange-red powder in 89% yield (1.44 g). Mp: 215-217 °C, decomposes at 230-236 °C; ^{1}H NMR (400 MHz, $CDCl_3$): δ 7.92 (s, 1H, Ar-*H*), 7.67 (s, 1H, Ar-*H*), 7.23 (s, 1H, Ar-*H*), 6.48 (s, 1H, Ar-*H*), 2.41 (s, 3H, Ar-COCH_3); ^{13}C {^{1}H} NMR (100 MHz, $CDCl_3$): δ 178.1, 167.7, 149.8, 148.6, 148.0, 142.5, 141.4, 131.7 (overlap), 131.0, 124.5, 111.8, 107.0, 20.7; MS (ESI−): *m/z* calcd for $[M - CH_3CO]^-$ $(C_{12}H_4O_3NCl_2)^-$ 280.0, found 279.7.

Synthesis of 4,6-Bis((bis(pyridin-2-ylmethyl)amino)methyl)-2,8-dichloro-7-hydroxy-3*H*-phenoxazin-3-one (ZR1, 8). DPA (0.13 g, 0.65 mmol) and paraformaldehyde (0.019 g, 0.65 mmol) were mixed in 20 mL of dry CH_3CN and heated to reflux for 30 min under nitrogen

atmosphere. To this clear solution, a suspension of compound **7** (0.042 g, 0.13 mmol) in 10 mL of dry CH_3CN and 2 mL of DCM was added dropwise over 5 min, and the mixture was then heated to reflux under nitrogen with stirring for 20 h. After cooling to room temperature, the solvent was removed under reduced pressure and the purple residue was dissolved in 100 mL of $CHCl_3$. The organic phase was washed with water (4 × 100 mL) and brine (100 mL). Concentrating the $CHCl_3$ solution to dryness yielded a dark blue solid, which was triturated with pentane/Et_2O 1:1 v/v (50 mL). Evaporation of the supernatant afforded a crude product, which was purified by semi-preparative reverse phase HPLC using the (A) water (0.1% v/v TFA) / (B) CH_3CN (0.1% v/v TFA) solvent system according to the following protocol: constant flow rate 3 mL min^{-1}; 5 min, isocratic flow 5% B; 20 min, linear gradient 5-35% B. The equivalent fractions from independent runs were combined and lyophilized to dryness. Triturating the solid with pentane/Et_2O 1:1 (10 mL) followed by drying to constant weight at 50-60 °C in vacuo afforded ZR1 (**8**) as a violet powder in 31% yield (28 mg). The purity was judged to be ~94% by analytical HPLC (Figure S16B), according to the protocol described above for ZBR4; retention time: 21.6 min. Mp: 154-158 °C (from $CHCl_3$); IR (KBr): 2924, 1682, 1443, 1348, 1207, 1139, 723 cm^{-1}; ^1H NMR (400 MHz, $CDCl_3$): δ 9.17 (br, 1H, Ar-O*H*), 8.58 (d, J = 5.0 Hz, 4H, Py-*H*), 7.71 (td, J = 7.7, 1.8 Hz, 4H, Py-*H*), 7.65 (s, 2H, Ar-*H*), 7.53 (d, J = 7.7 Hz, 4H, Py-*H*), 7.23 (m, 4H, Py-*H*), 4.68 (s, 4H, Ar-CH_2), 4.56 (s, 8H, Py-CH_2); ^{13}C {^1H} NMR (100 MHz, $CDCl_3$): δ 173.1, 153.2, 148.8, 145.8, 138.0, 131.5 (overlap), 130.55, 124.1, 123.7, 107.4, 58.5, 49.5; HRMS (ESI+): *m/z* calcd for $[M + H]^+$ $(C_{38}H_{32}O_3N_7Cl_2)^+$ 704.1944, found 704.1957.

Spectroscopic Methods. All aqueous solutions were prepared with deionized water (Millipore). Piperazine-*N,N'*-bis(2-ethanesulfonic acid) (PIPES) and 99.999% KCl were purchased from Calbiochem. High-purity 99.999% $ZnCl_2$ and 0.1 M aq. $ZnSO_4$ volumetric solution were supplied by Aldrich. Stock solutions of ZBR4 (0.3−1.0 mM in deionized water with 0.1% TFA v/v) and ZR1 (2.0 mM in spectroscopic grade DMSO) were stored at −40 °C in 50 μL aliquots, and thawed immediately before use. All spectroscopic measurements were conducted in aqueous buffer (50 mM PIPES, 100 mM KCl, pH 7.0), except the pK_a titrations, which were conducted in aqueous buffers containing 100 mM KCl and 20 mM acetic acid. The buffer solutions were pretreated with Chelex resin (Bio-Rad) to remove residual metal ions in solution. The pH measurements were performed with a Mettler Toledo FE20 pH meter. All

measurements were conducted at 25.0 or 37.0 °C, maintained by a circulating water bath. Extinction coefficients were determined in the 0.1−5 μM range in buffer solutions at pH 7.0 with 10 μM EDTA for the metal-free form or with 50 μM $ZnCl_2$ for the metal-bound form of the sensor. Fluorescence quantum yields were determined using 0.1−5 μM sensor in buffer solutions at pH 7.0. The quantum yield calculations were standardized to resorufin, with a reported quantum yield of 0.74 at pH 9.5.[2] In all cases, excitation was provided at 560 nm and the fluorescence emission spectra were integrated from 570 to 750 nm. All measurements were repeated in triplicate.

Cell Culture and Staining Procedures. HeLa cells were cultured in Dulbecco's Modified Eagle Medium (DMEM, GIBCO), supplemented with 10% heat-deactivated fetal bovine serum (FBS) and 1% penicillin/streptomycin, at 37 °C in a humidified atmosphere with 5% CO_2. Cells were plated in 35 mm glass-bottom, poly-D-lysine coated culture dishes with 14 mm opening (MatTek) 24−48 h before imaging. All the cells used were at the passage number from 5 to 15, and the experiments were repeated on cells from at least three different passages. A confluence level of 30−50% was reached at imaging. Cells were incubated with the sensor and organelle stains at 37 °C for 15−20 min before mounting to the microscope. The growth medium was replaced with 2 mL of fresh dye- and serum-free DMEM containing 1 μM ZBR4 or 2 μM ZR1 and selected organelle stains before incubation. The organelle-specific dyes employed were: Hoechst 33258 (Invitrogen, final concentration 10 μM), MitoTracker Green (Invitrogen, final concentration 0.25−0.5 μM), ER-Tracker Green (Invitrogen, final concentration 1 μM), and ER-Tracker Blue-White DPX (Invitrogen, final concentration 2 μM). Cells were rinsed with sterile PBS buffer (2 × 2 mL) and then with dye- and serum-free DMEM (2 mL) to remove excess unbound dyes. Cells were bathed in 2 mL of dye- and serum-free DMEM before mounting on the microscope. After the initial sets of images were acquired, Zn^{2+}-induced fluorescence changes were measured by replacing the medium with 2 mL of a pre-mixed solution of 50 μM $ZnCl_2$ and 100 μM sodium pyrithione (2-pyridinethiol-1-oxide) in dye- and serum-free DMEM. Finally, the Zn^{2+}-containing medium was removed and 2 mL of a 50 μM *N*,*N*,*N'*,*N'*-tetrakis(2-pyridylmethyl)-ethylenediamine (TPEN) solution in dye- and serum-free DMEM was applied to the Petri dish to reverse the Zn^{2+}-induced fluorescence response.

Fluorescence Microscopy. Fluorescence imaging experiments were carried out on a Zeiss Axiovert 200M inverted epifluorescence microscope equipped with a Hamamatsu EM-CCD C9100 digital camera and an MS200 XY Piezo Z stage (Applied Scientific Instruments, Inc.). An XCite 120 metal halide lamp (EXFO) was used as the light source. Zeiss standard filter sets 49, 38 HE, and 43 HE were employed for imaging Hoechst 33258/ER-Tracker Blue-White DPX, MitoTracker Green and ZBR4/ZR1 dyes, respectively. The microscope was operated with the aid of the Volocity software (version 6.01, Improvision). The exposure times for the acquisition of images of a given culture dish were kept constant for each channel. The quantification of fluorescence intensity was performed with ImageJ (version 1.47, NIH). For each measurement, the whole cell was selected as region of interest and the integrated fluorescence from the background region was subtracted from the integrated fluorescence intensity of the cell body region. In order to evaluate co-localization of the sensors with organelle-specific stains, Pearson's correlation coefficients were calculated for individual cells with the PSC Colocalization plugin of ImageJ,[3] choosing in each case the maximum background fluorescence signal as threshold. The images employed in co-localization studies were deconvoluted using the Volocity iterative restoration algorithms.

Study of pH-Dependent Fluorescence. The apparent pK_a values were measured by integrating the fluorescence intensity of emission spectra recorded in pH increments of 0.25 and 0.5 for ZBR4 and ZR1, respectively, in the 1 to 10 range. For each data point, 20−30 mL of a buffered aqueous stock solution containing 100 mM KCl and 20 mM sodium acetate were prepared by adjusting the pH to the desired value with 1.0 and 0.1 M aq. HCl, or 1.0 and 0.1 M aq. KOH. 1 μM aliquots of the sensors (2 mL total volume) were then prepared in each of the pH-buffered aqueous solutions, and the absorption and emission spectra at each pH value were recorded for both metal-free and Zn^{2+}-bound form (following addition of 20 μM $ZnSO_4$). Measurements for the metal-free form of ZBR4 were repeated in triplicate. Emission spectra were integrated from 570 to 750 nm. The integrated data were normalized (F/F_{max}), plotted against the pH value, and fitted to the nonlinear expression below to calculate the pK_a values for ZBR4. A similar two-term expression[4] was used to determine two apparent pK_a values for ZR1. The non-linear fit was performed with the OriginPro 8 software (version 8.0724, OriginLab Corporation).

$$\frac{F - F_0}{F_{max} - F_0} = \frac{\Delta F_{1max}}{(1+10^{(pH-pK_{a1})})} + \frac{\Delta F_{2max}}{(1+10^{(pH-pK_{a2})})} + \frac{\Delta F_{3max}}{(1+10^{(pH-pK_{a3})})}$$

In the above equation, F_{max} is the maximum normalized emission intensity ($F_{max} = 1$), F_0 is the minimum normalized emission intensity obtained for pH = 1, and ΔF_{1max}, ΔF_{2max}, and ΔF_{3max} are the maximum fluorescence changes associated with the corresponding pK_a values. The apparent pK_a values obtained for ZBR4 were: pK_{a1} = 6.26 ± 0.05, pK_{a2} = 3.24 ± 0.14, pK_{a3} = 2.14 ± 0.09, R^2 = 0.9933.

Metal Selectivity and Apparent Dissociation Constants. The metal selectivity profiles of ZBR4 and ZR1 were determined by comparing the fluorescence emission spectra of 1.0 μM solution of the sensors with 1 μM EDTA in aqueous buffer at pH 7.0, before and after treatment with NaCl, $CaCl_2$, $MgCl_2$, $MnCl_2$, $FeCl_2$ (freshly prepared), $CoCl_2$, $NiCl_2$, $CuCl_2$ or $CdCl_2$ stock solutions in deionized water, for a final cation concentration of 20 μM (1 mM for Na^+, Ca^{2+} and Mg^{2+}). The fluorescence was then measured after subsequent addition of $ZnSO_4$ for a final concentration of 20 μM. In each case, the integrated fluorescence emission spectra were normalized with respect to the metal-free control spectrum, arbitrarily assigned as unity. The apparent Zn^{2+} dissociation constants for the two binding sites of ZBR4 were determined by 1 or 2 μL incremental addition of aq. 0.1 M $ZnSO_4$ to 2.0 mL of a 1 μM sensor solution in aqueous buffer at pH 7.0, containing 1 mM of ethylene glycol-bis(2-aminoethylether)-*N*,*N*,*N'*,*N'*-tetraacetic acid (EGTA). The free Zn^{2+} concentrations in the 1 mM EGTA buffer at selected total Zn^{2+} concentrations were calculated with the online MaxChelator software suite (http://maxchelator.stanford.edu/) and are provided in Table S1. Excitation was performed at 560 nm, and the response (R) was quantified by integrating the emission intensity from 570 to 750 nm, subtracting the initial spectrum (0 mM total Zn^{2+}) and normalizing to the maximum fluorescence turn-on, achieved for the final spectrum at 1.1 mM total Zn^{2+} concentration (100 μM free Zn^{2+}). The response was then plotted vs $[Zn^{2+}]_{free}$ and fitted to the equation:[5]

$$R = (P \times [Zn^{2+}]_{free}) / (K_d + [Zn^{2+}]_{free})$$

The fit parameter obtained were P = 0.93 and R^2 = 0.993.

Table S1. Total and free Zn^{2+} concentrations in 1 mM EGTA aqueous buffer

$[Zn^{2+}]_{total}$, mM	0.05	0.1	0.15	0.2	0.3	0.4	0.5	0.6	0.7	0.8	0.9	0.95	1.0	1.1
$[Zn^{2+}]_{free}$, nM	0.29	0.62	0.99	1.4	2.4	3.74	5.61	8.42	13.1	22.5	50.5	106.6	2400	10^5

Table S2. Photophysical parameters of ZBR4 and ZR1 in aqueous buffer, pH = 7.0

	Metal-free				**Zn^{2+}-saturated**			
	absorption		emission		absorption		emission	
probe	λ_{max} (nm)	$\varepsilon \times 10^{-4}$ (M^{-1} cm^{-1})	λ_{max} (nm)	Φ (%)	λ_{max} (nm)	$\varepsilon \times 10^{-4}$ (M^{-1} cm^{-1})	λ_{max} (nm)	Φ (%)
ZBR4	569	2.84 ± 0.17	629	3.55 ± 0.2	573	3.67 ± 0.12	631	50.25 ± 1.1
ZR1	606	5.43 ± 0.02	607	1.02 ± 0.01	593	5.77 ± 0.01	611	42.05 ± 1.6

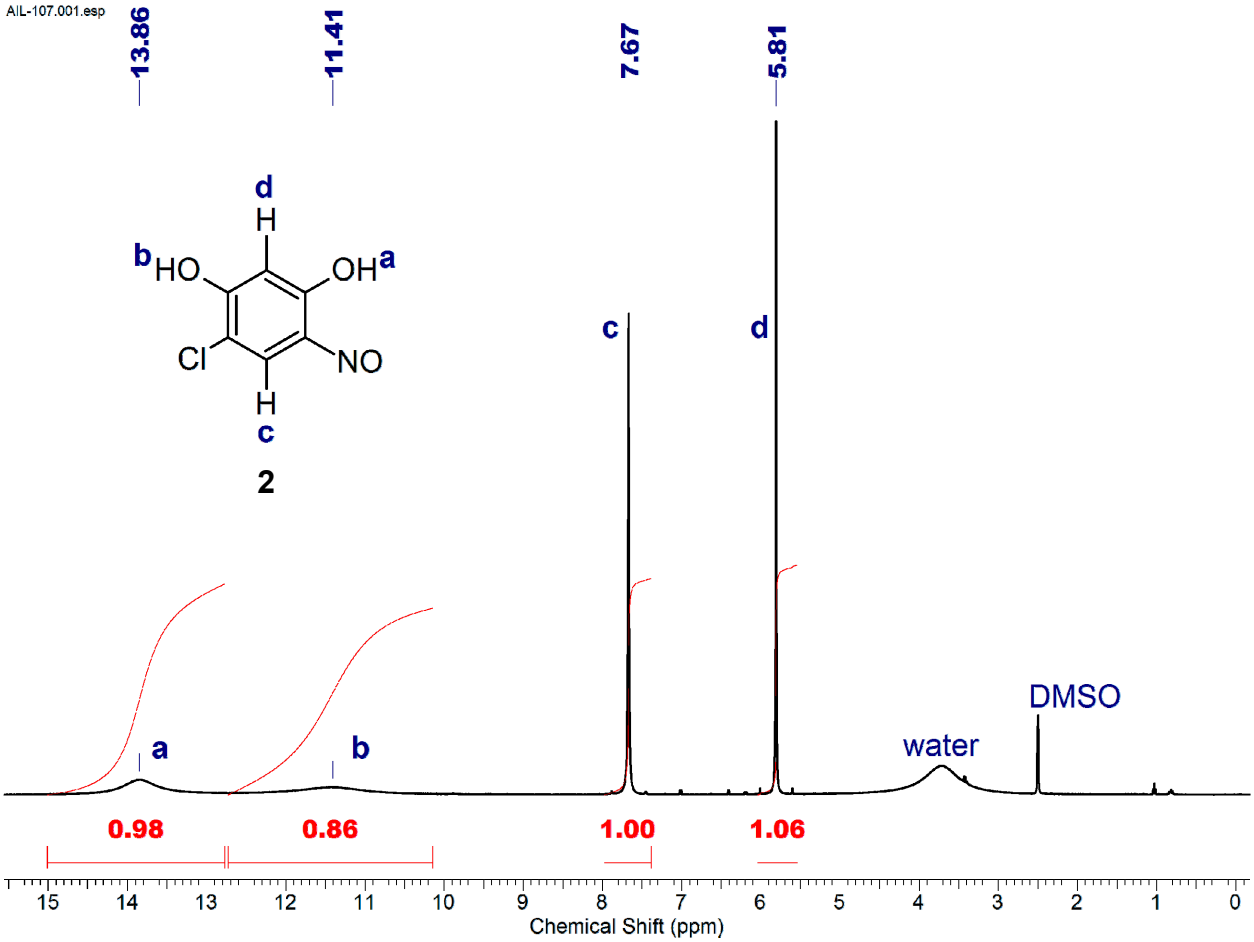

Figure S1. ^{1}H NMR spectrum of compound **2** (400 MHz, $(CD_3)_2SO$).

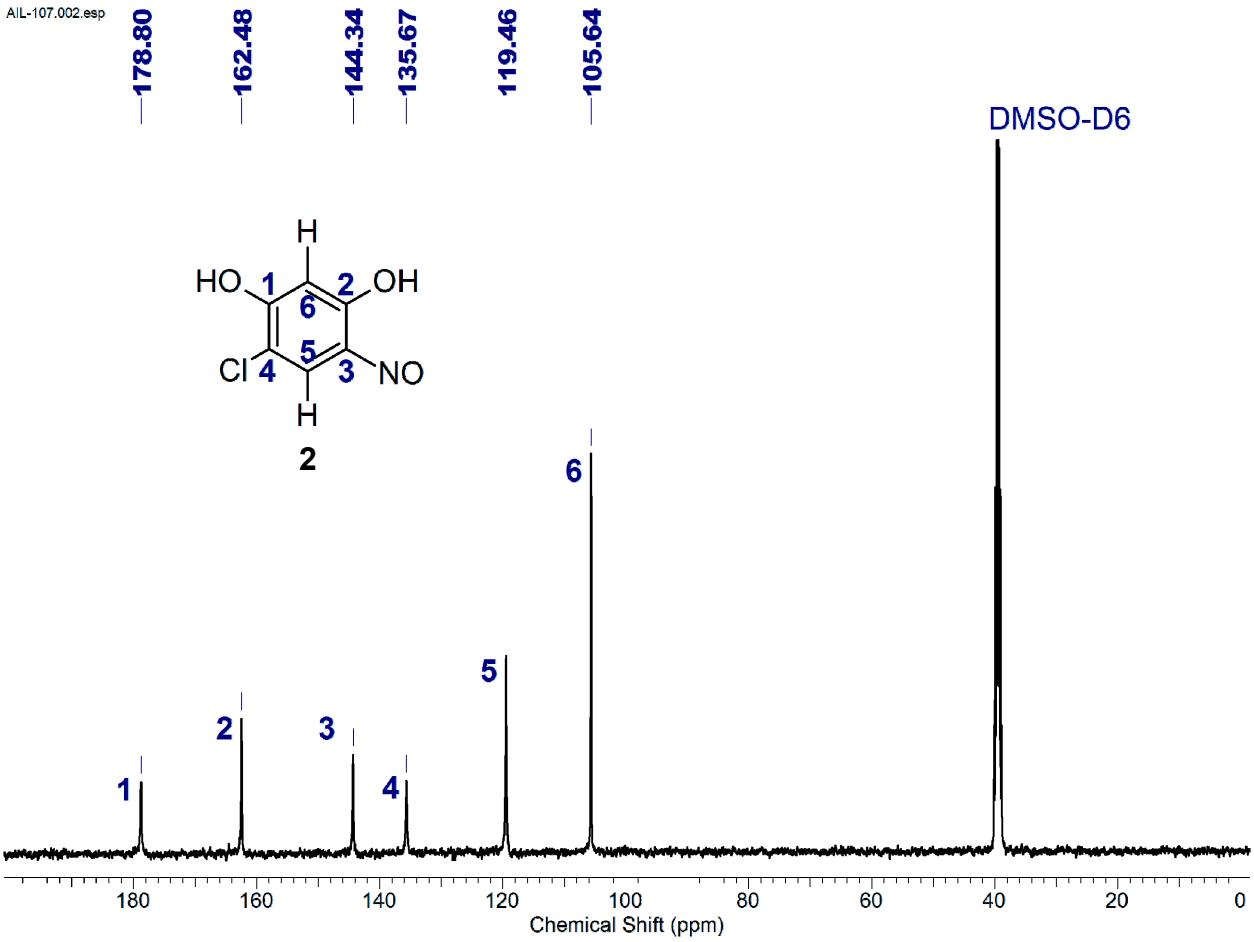

Figure S2. ^{13}C {^{1}H} NMR spectrum of compound **2** (100 MHz, $(CD_3)_2SO$).

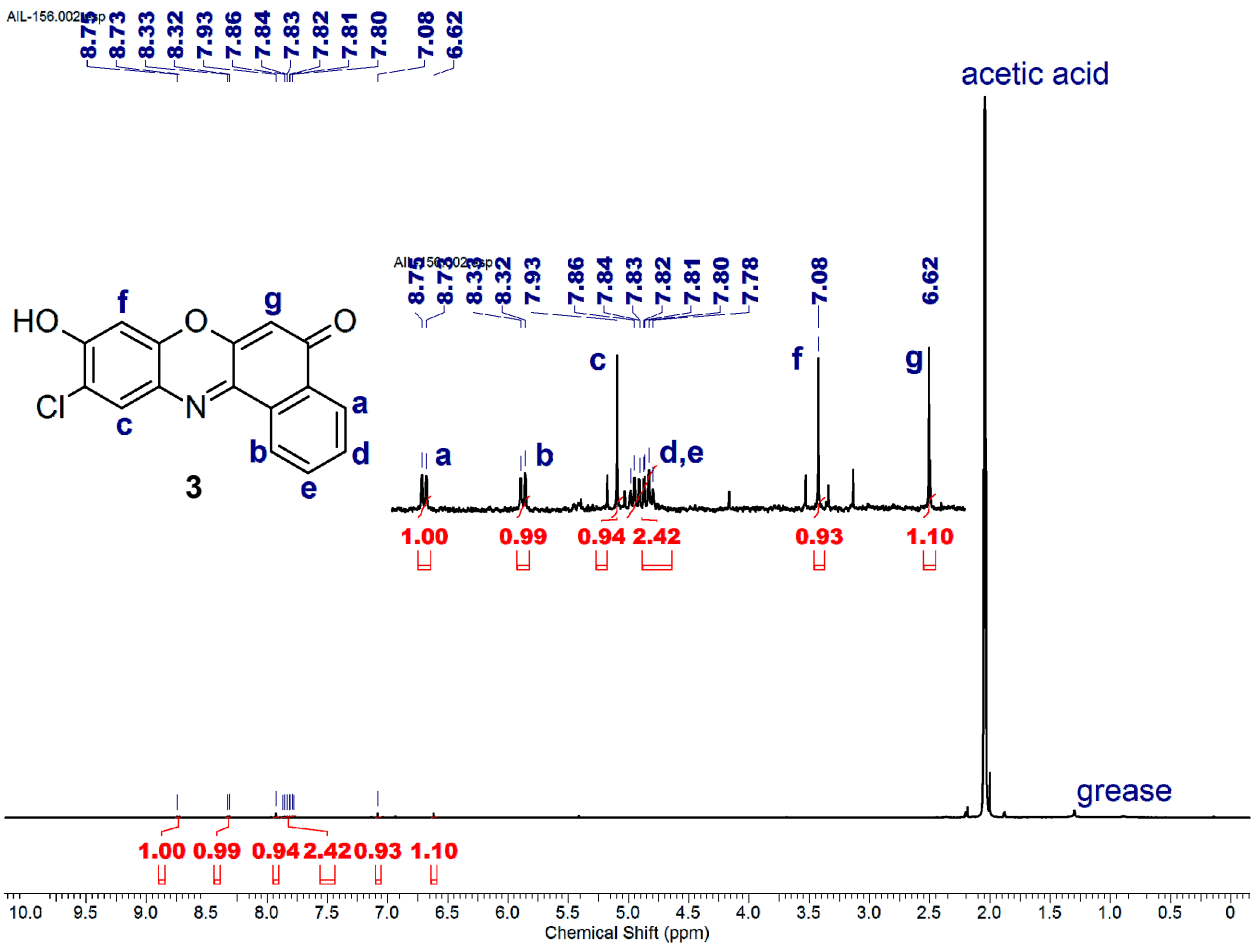

Figure S3. ^{1}H NMR spectrum of compound **3** (400 MHz, CD_3COOD).

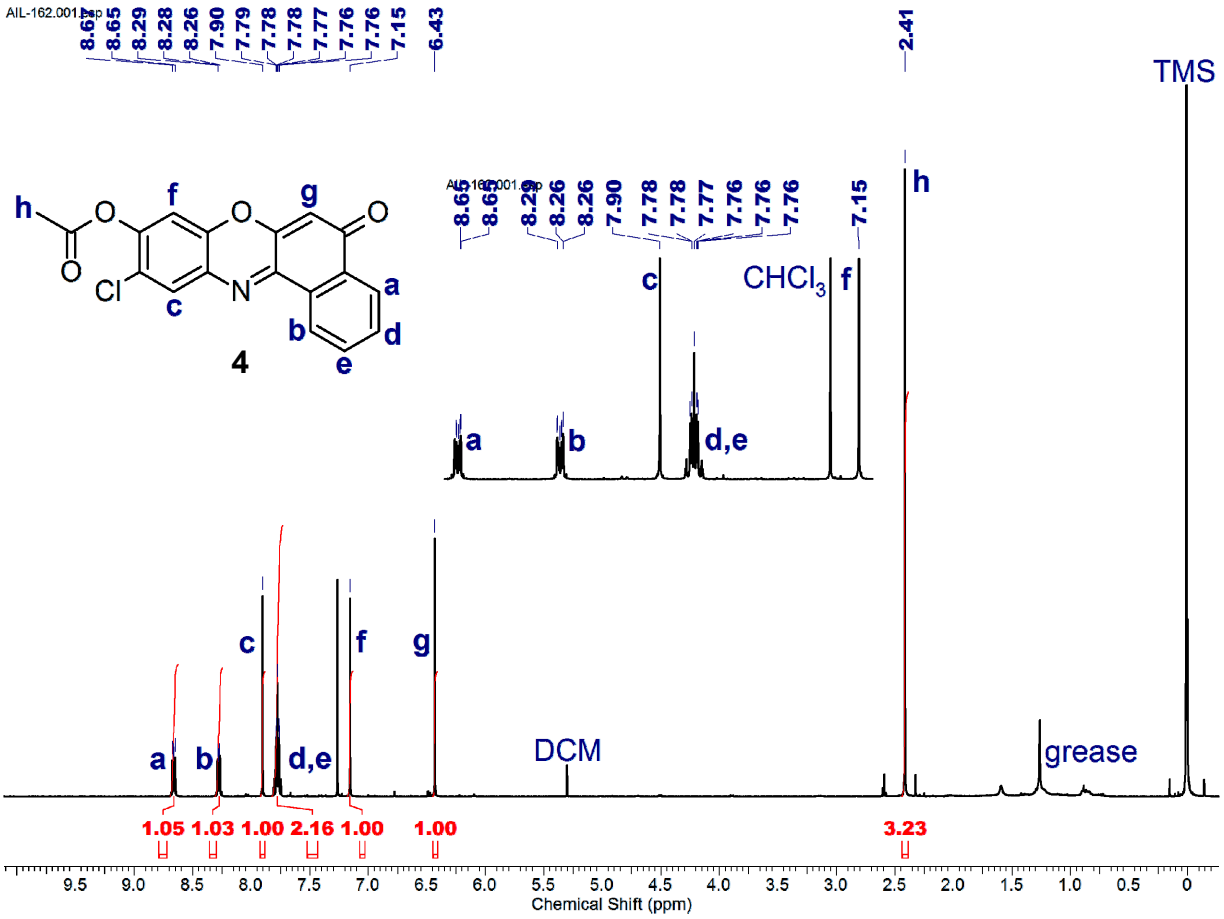

Figure S4. ^{1}H NMR spectrum of compound **4** (400 MHz, $CDCl_3$).

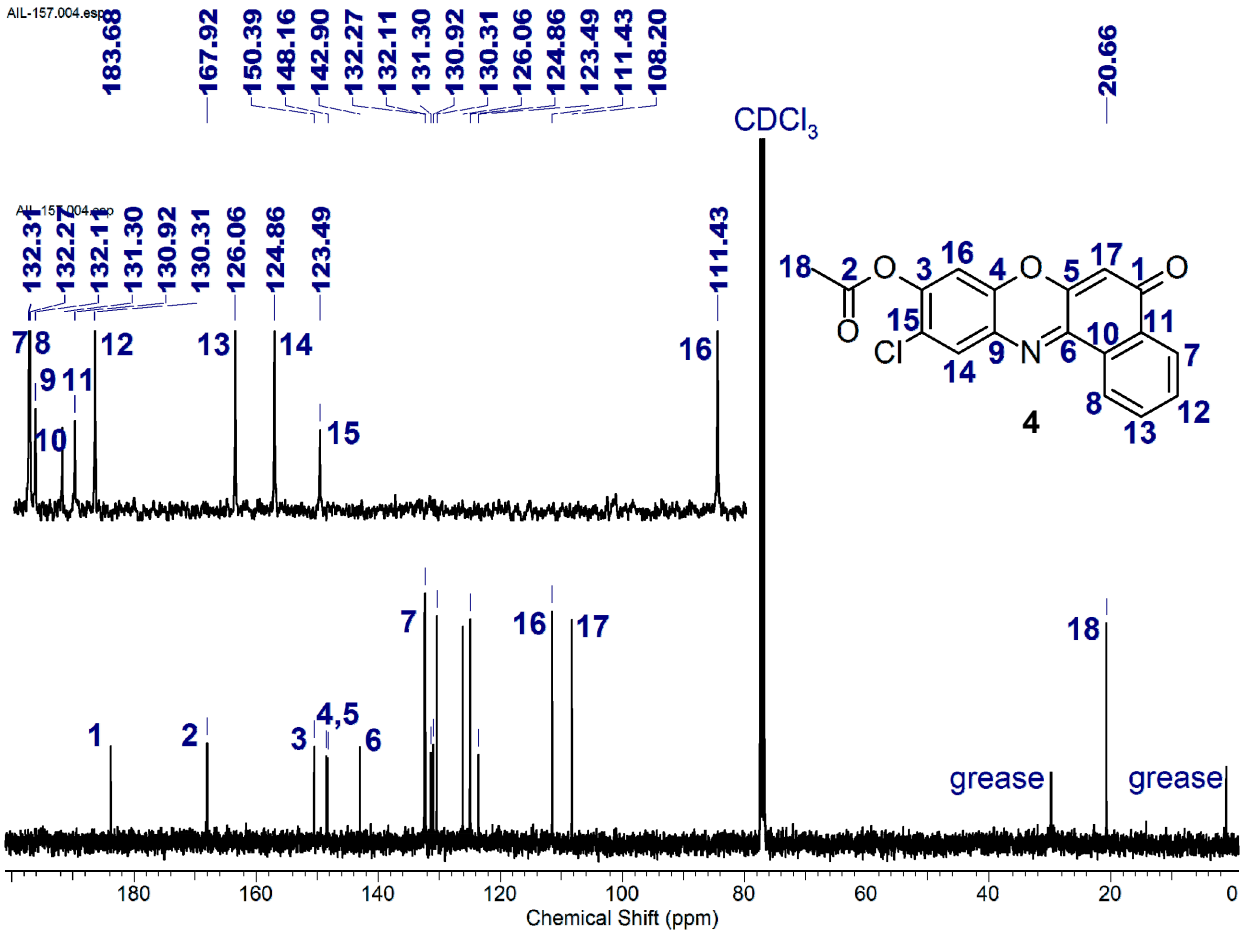

Figure S5. ^{13}C {^{1}H} NMR spectrum of compound **4** (100 MHz, $CDCl_3$).

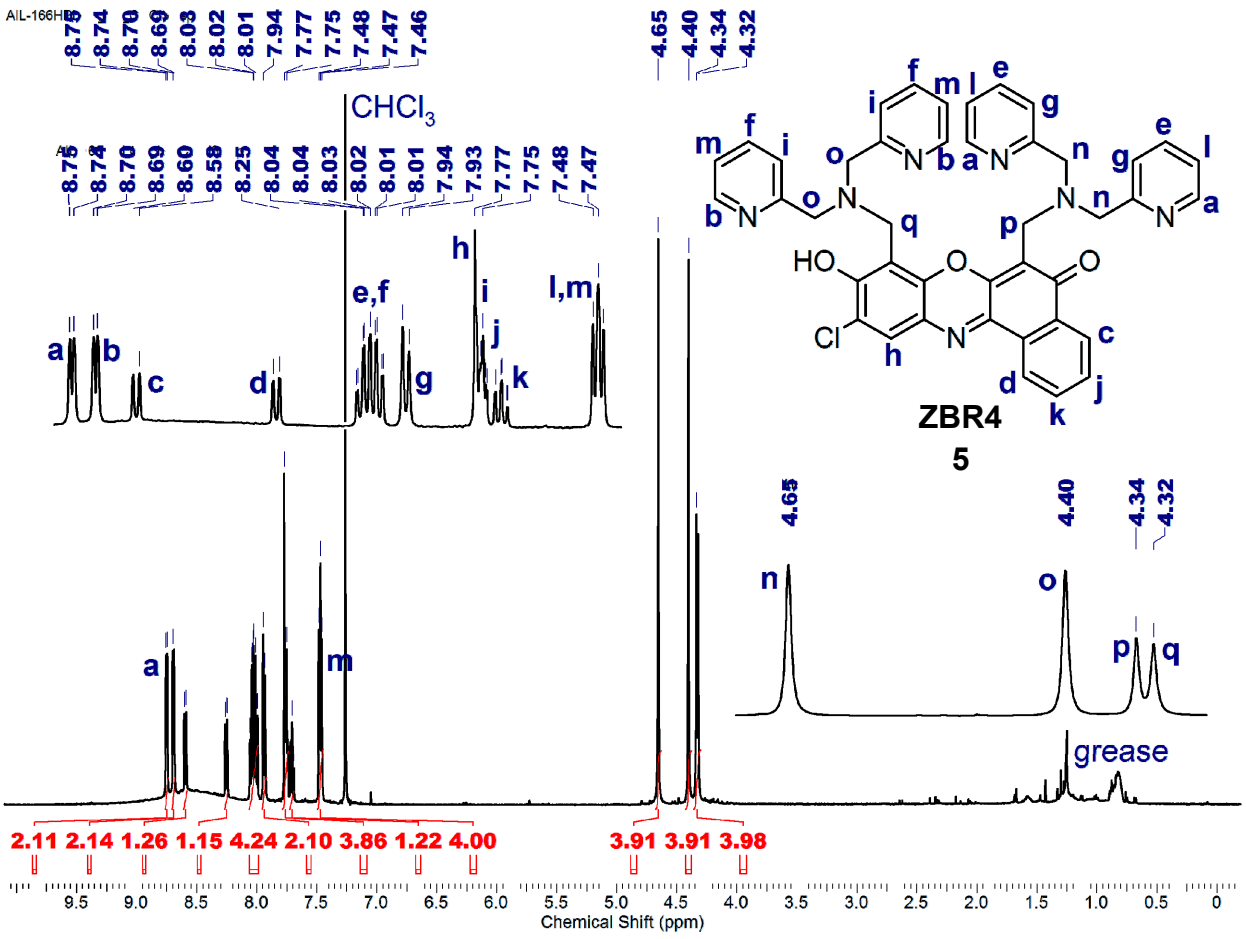

Figure S6. ^{1}H NMR spectrum of compound **5**, ZBR4 (500 MHz, $CDCl_3$).

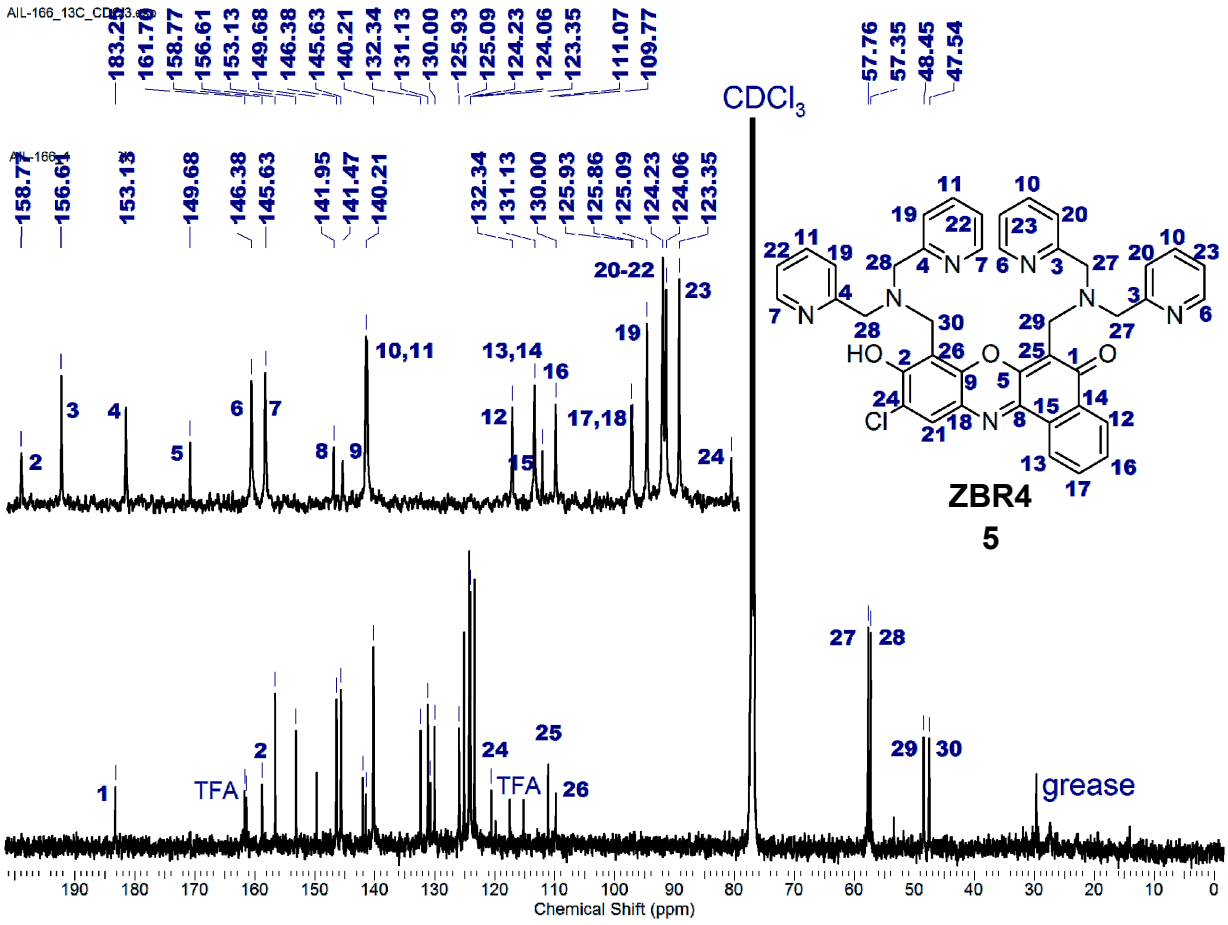

Figure S7. ^{13}C {^{1}H} NMR spectrum of compound **5**, ZBR4 (125 MHz, $CDCl_3$).

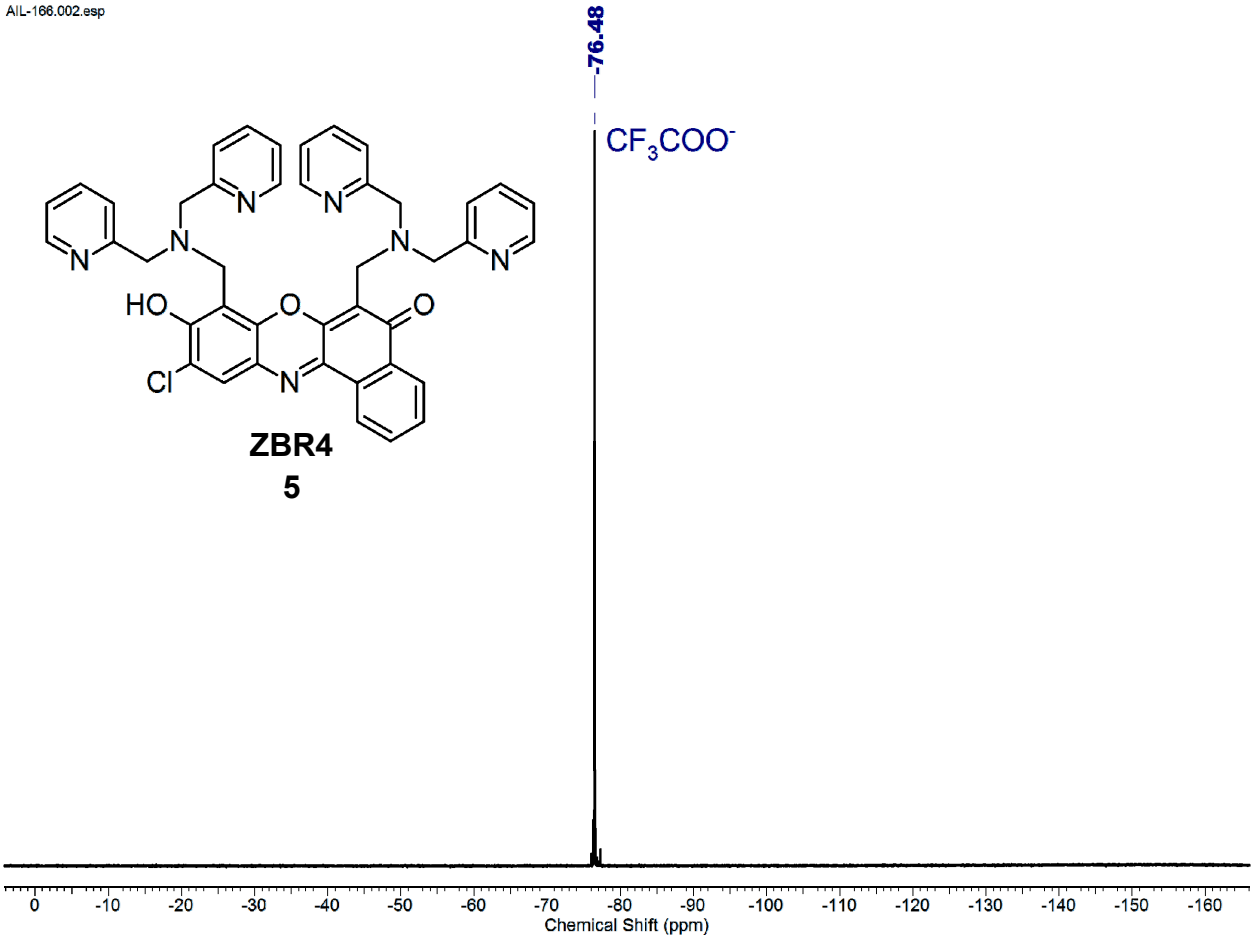

Figure S8. ^{19}F NMR spectrum of compound **5**, ZBR4 (376 MHz, $CDCl_3$).

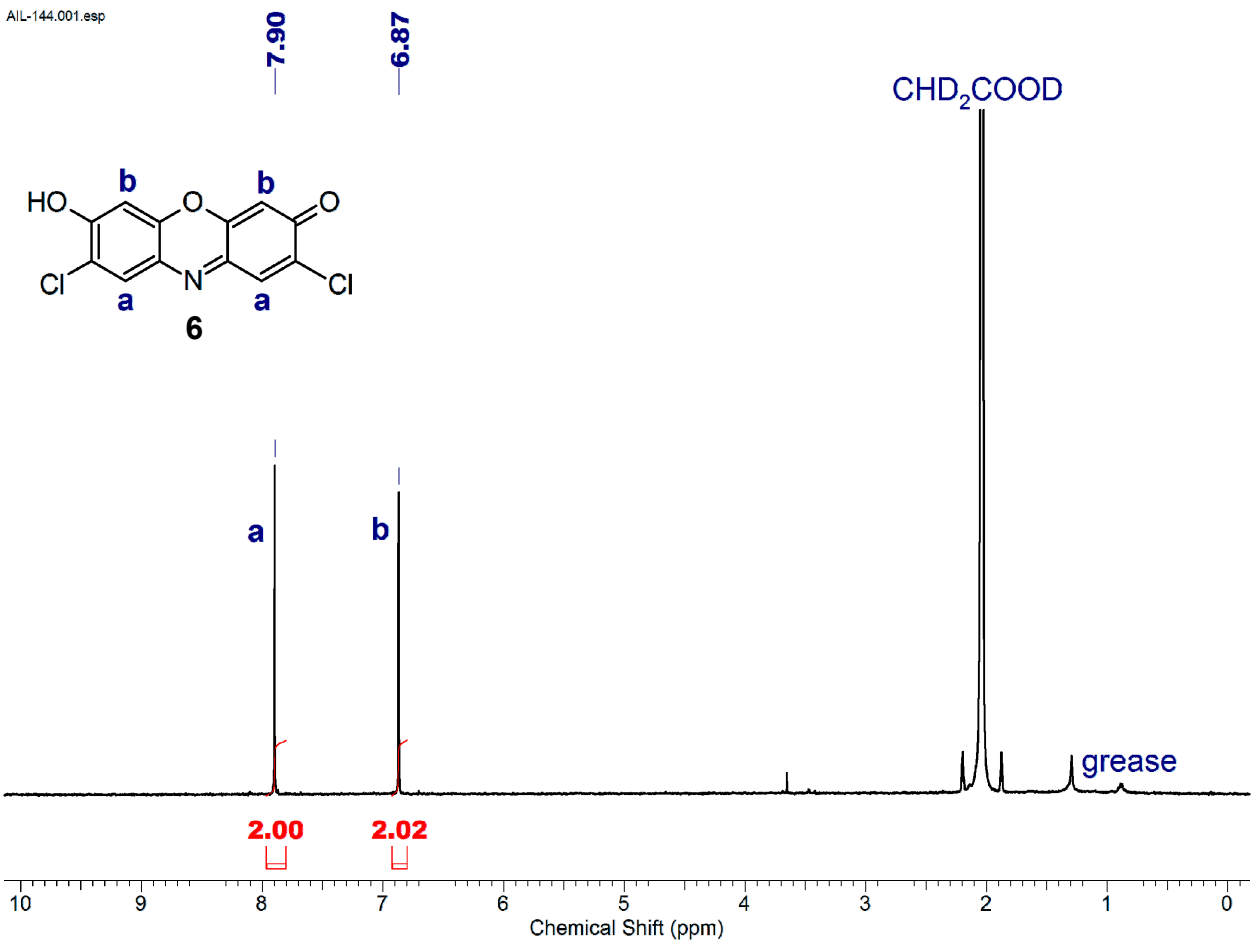

Figure S9. ^{1}H NMR spectrum of compound **6** (400 MHz, CD_3COOD).

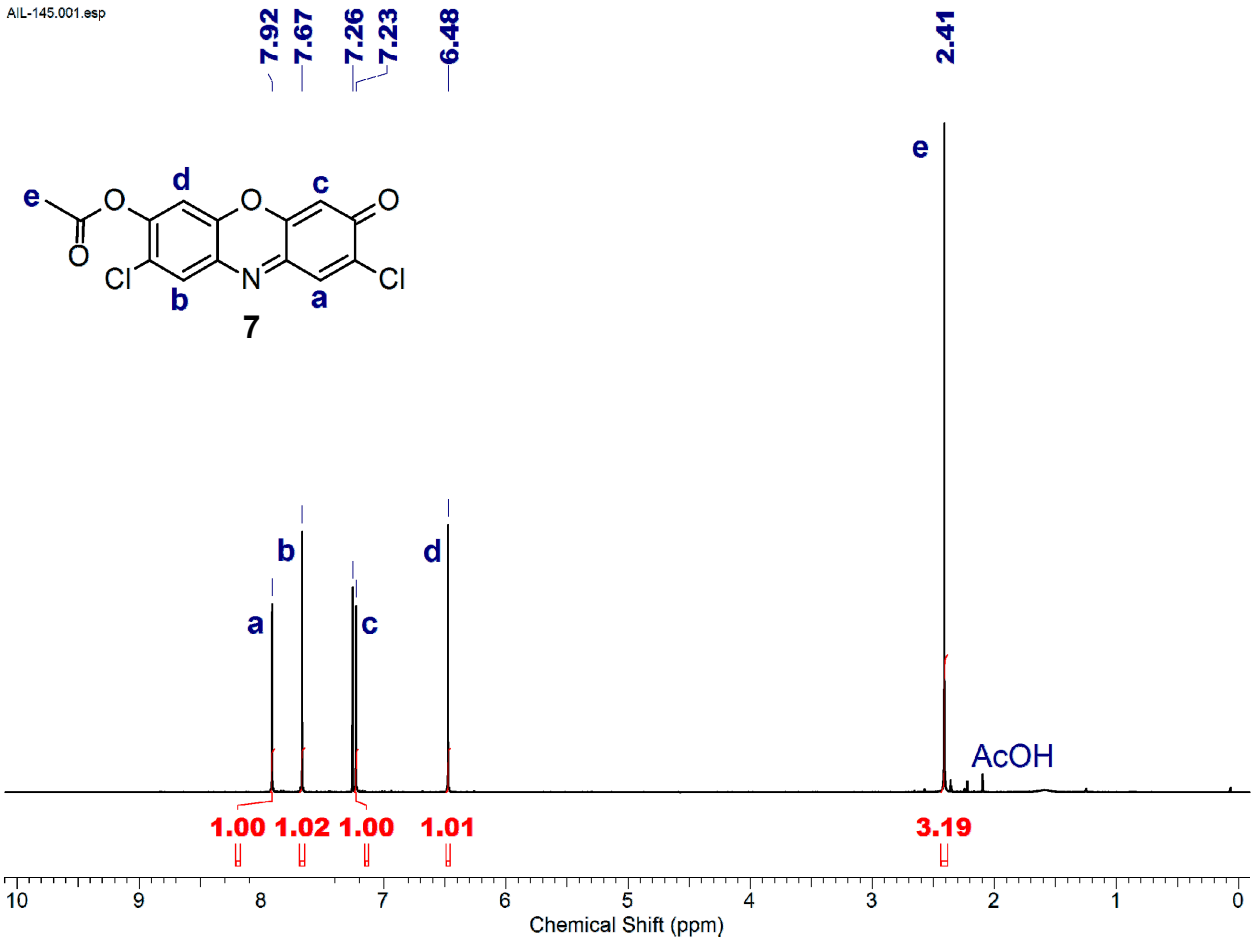

Figure S10. ^{1}H NMR spectrum of compound **7** (400 MHz, $CDCl_3$).

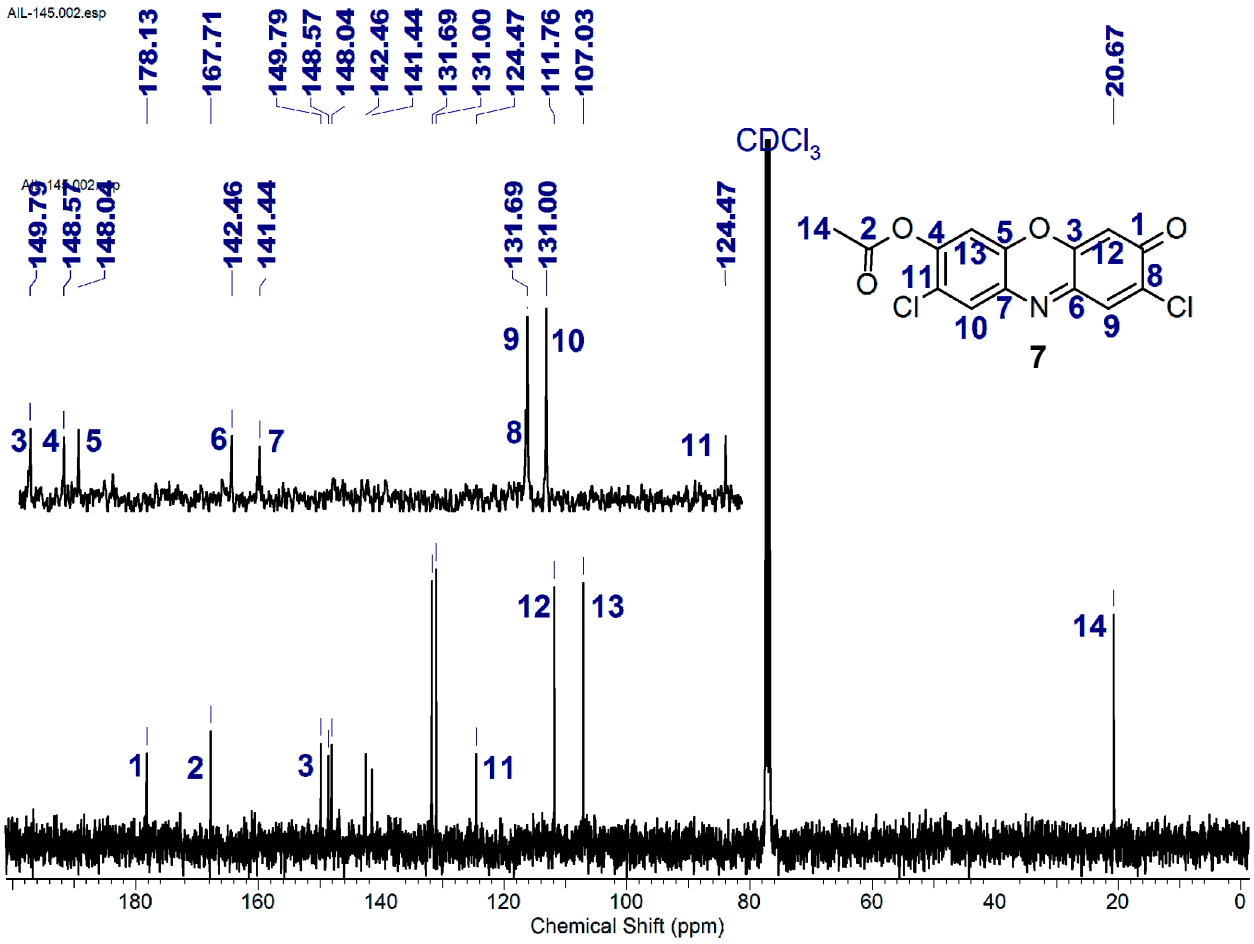

Figure S11. ^{13}C {^{1}H} NMR spectrum of compound **7** (100 MHz, $CDCl_3$).

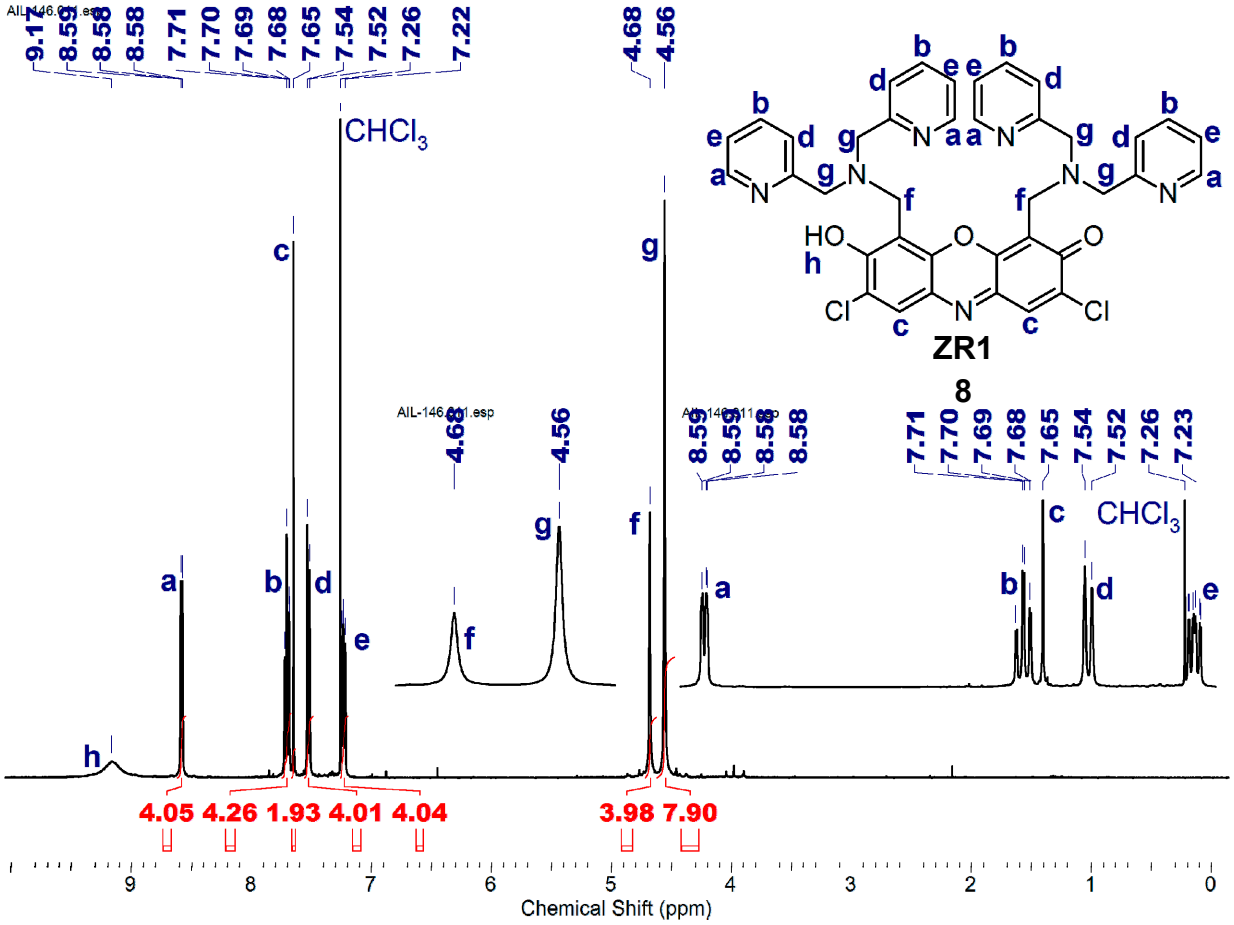

Figure S12. ^{1}H NMR spectrum of compound **8**, ZR1 (400 MHz, $CDCl_3$).

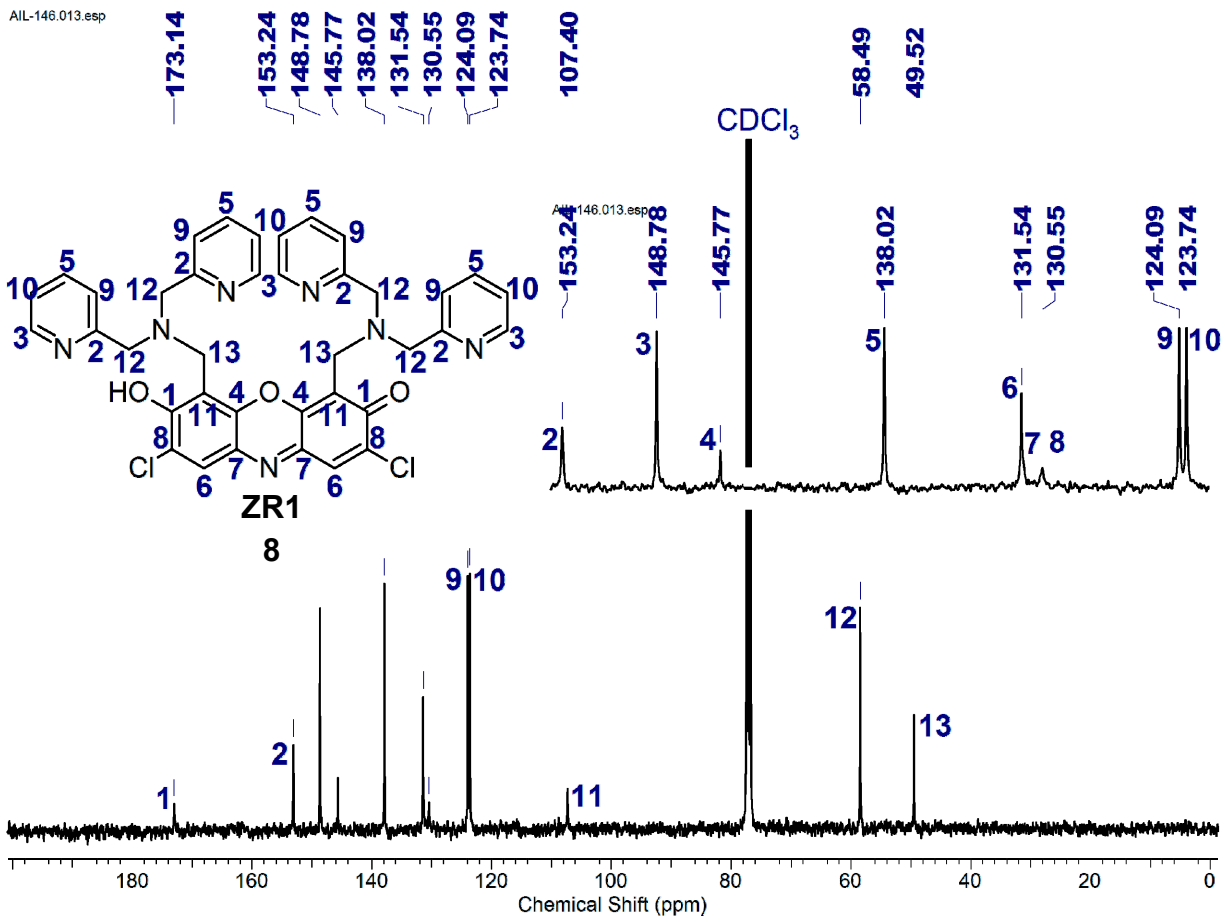

Figure S13. ^{13}C $\{^{1}H\}$ NMR spectrum of compound **8**, ZR1 (100 MHz, $CDCl_3$).

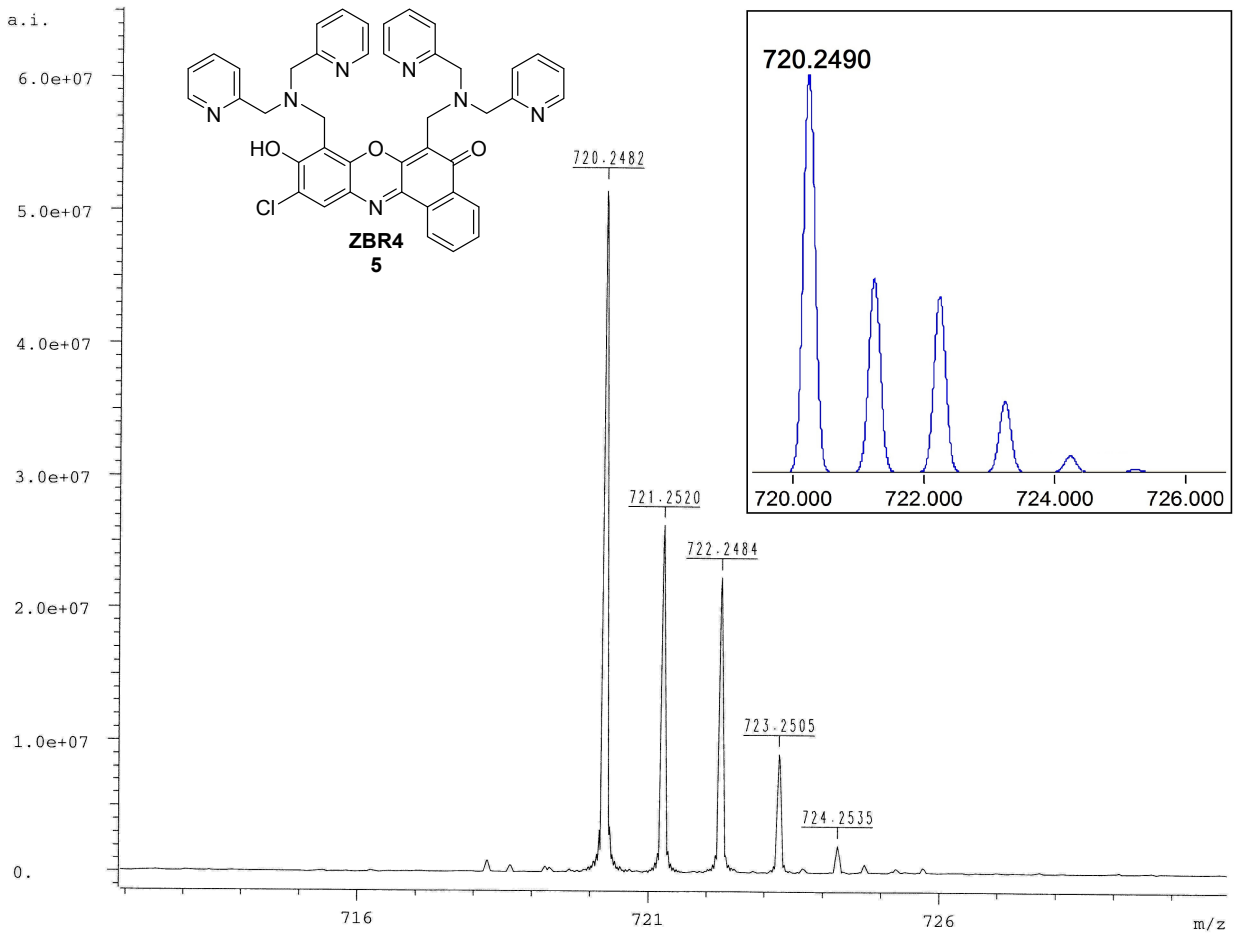

Figure S14. High-resolution mass spectrum (ESI+) of ZBR4 (**5**). Inset: calculated isotope pattern and exact mass.

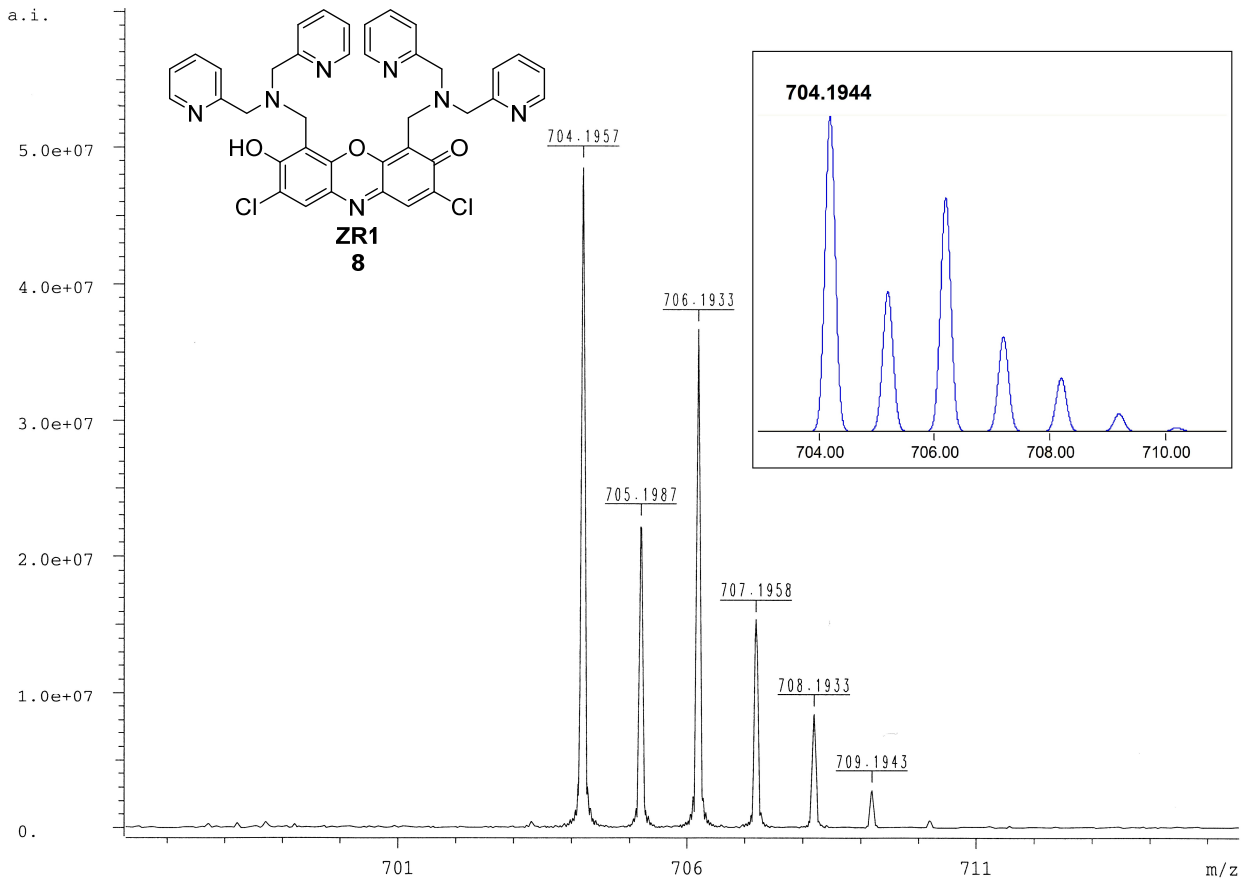

Figure S15. High-resolution mass spectrum (ESI+) of ZR1 (**8**). Inset: calculated isotope pattern and exact mass.

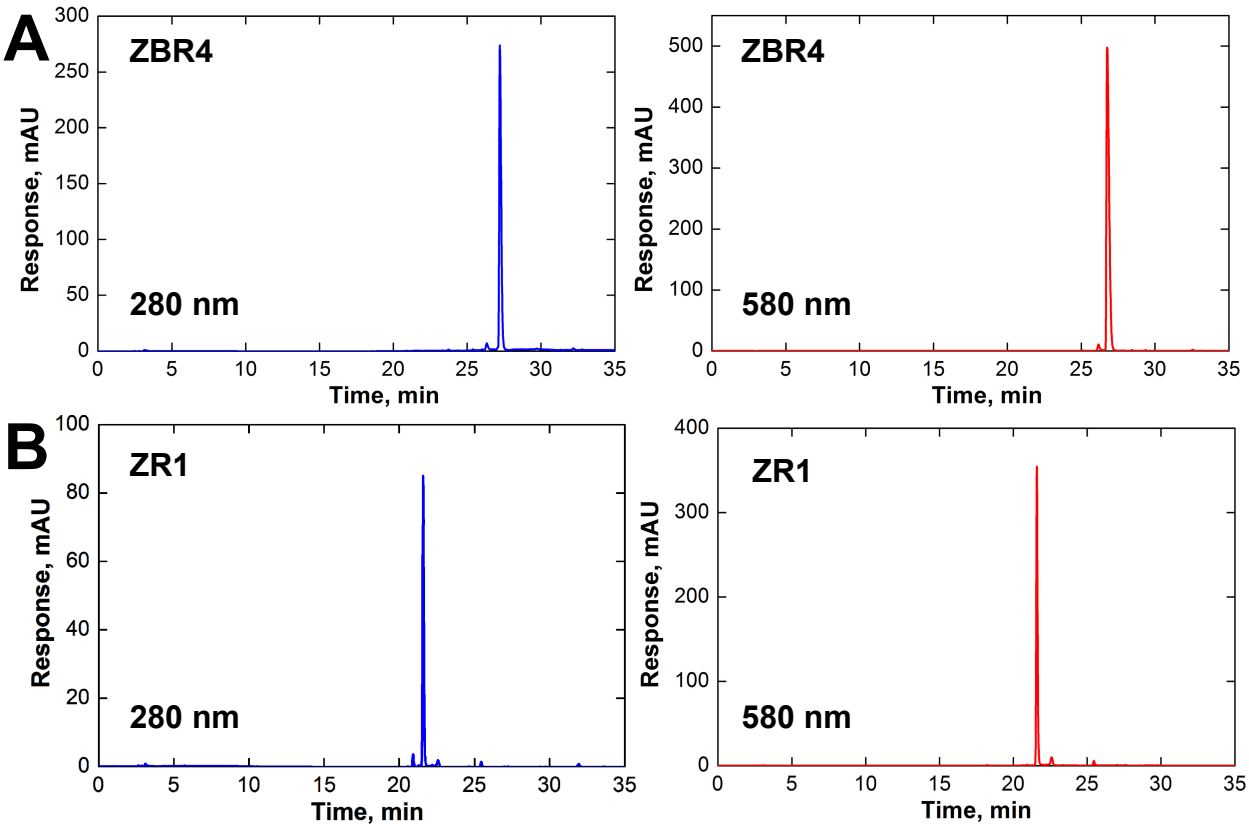

Figure S16. Analytical HPLC traces of (A) ZBR4 and (B) ZR1, detected by the signals at 280 and 580 nm.

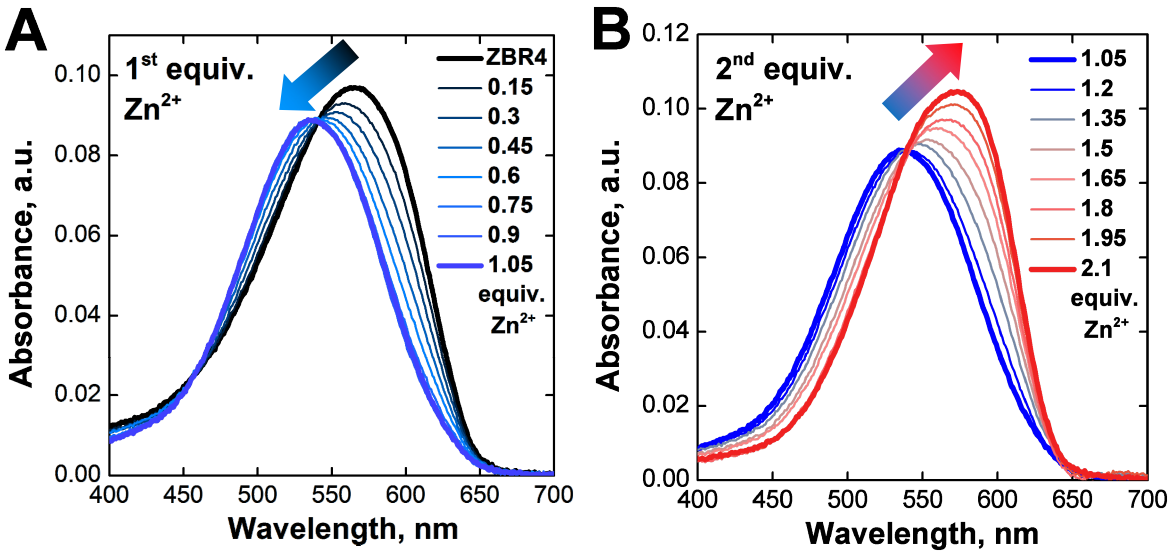

Figure S17. Electronic absorption spectra of 4 μM ZBR4 recorded upon addition of (A) first and (B) second equivalent of Zn^{2+} ($ZnSO_4$, 25 °C, 100 mM KCl, 50 mM PIPES, pH 7.0).

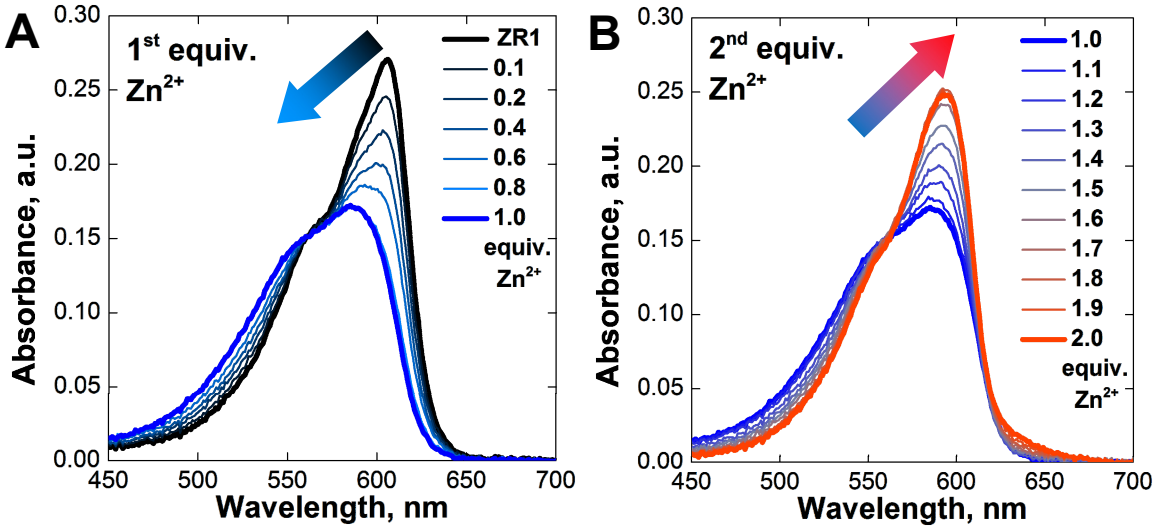

Figure S18. Electronic absorption spectra of 5 μM ZR1, recorded upon incremental addition of (A) first and (B) second equivalent of Zn^{2+} ($ZnCl_2$, 25 °C, 100 mM KCl, 50 mM PIPES, pH 7.0).

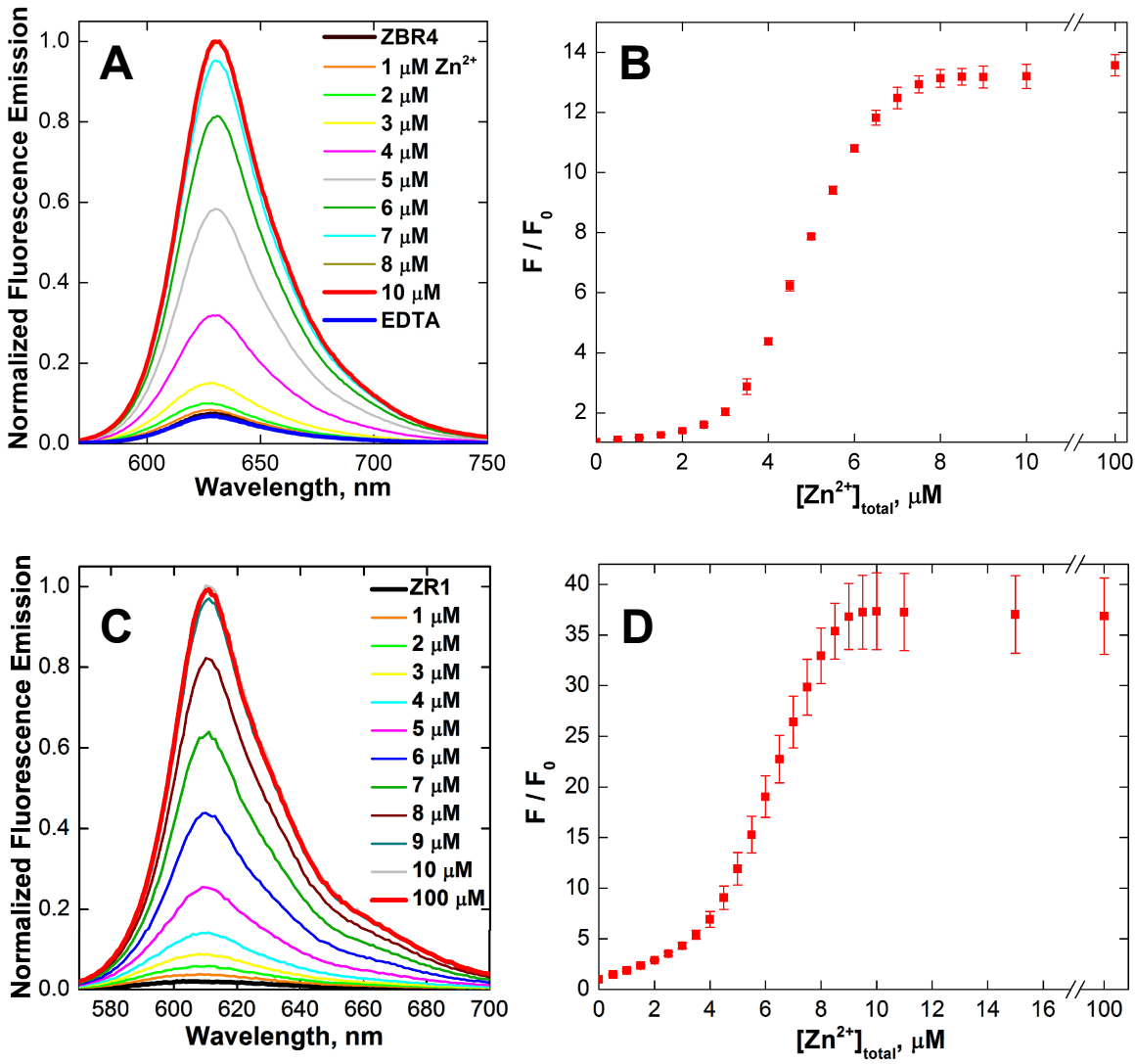

Figure S19. Left: normalized fluorescence emission spectra of (A) ZBR4 and (C) ZR1, recorded at increasing total concentrations of Zn^{2+}. Right: normalized integrated fluorescence emission of (B) ZBR4 and (D) ZR1 vs total Zn^{2+} concentration in aqueous buffer (4 μM ZBR4, 5 μM ZR1, $ZnCl_2$, 25 °C, 100 mM KCl, 50 mM PIPES, pH 7.0, λ_{ex} = 560 nm).

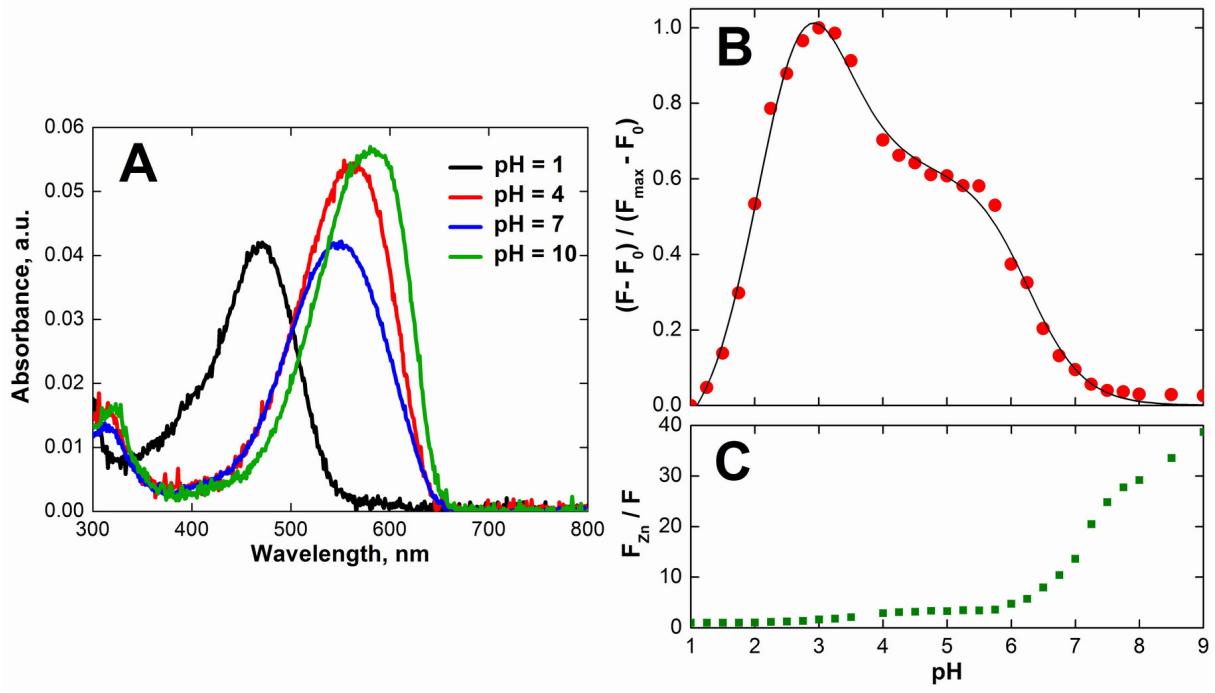

Figure S20. Effect of pH on a 1 μM aqueous solution of ZBR4 (25 °C, 100 mM KCl, 20 mM AcONa). (A) Representative absorption spectra at different pH values. (B) Normalized integrated fluorescence emission vs pH, showing the nonlinear fit (continuous line) to the experimental data (red circles) used to determine the apparent pK_a values. (C) Increase in integrated fluorescence emission vs pH upon addition of 50 μM $ZnSO_4$; for each pH value, the Zn^{2+}-induced response was normalized to the emission of the metal-free sensor. λ_{ex} = 560 nm.

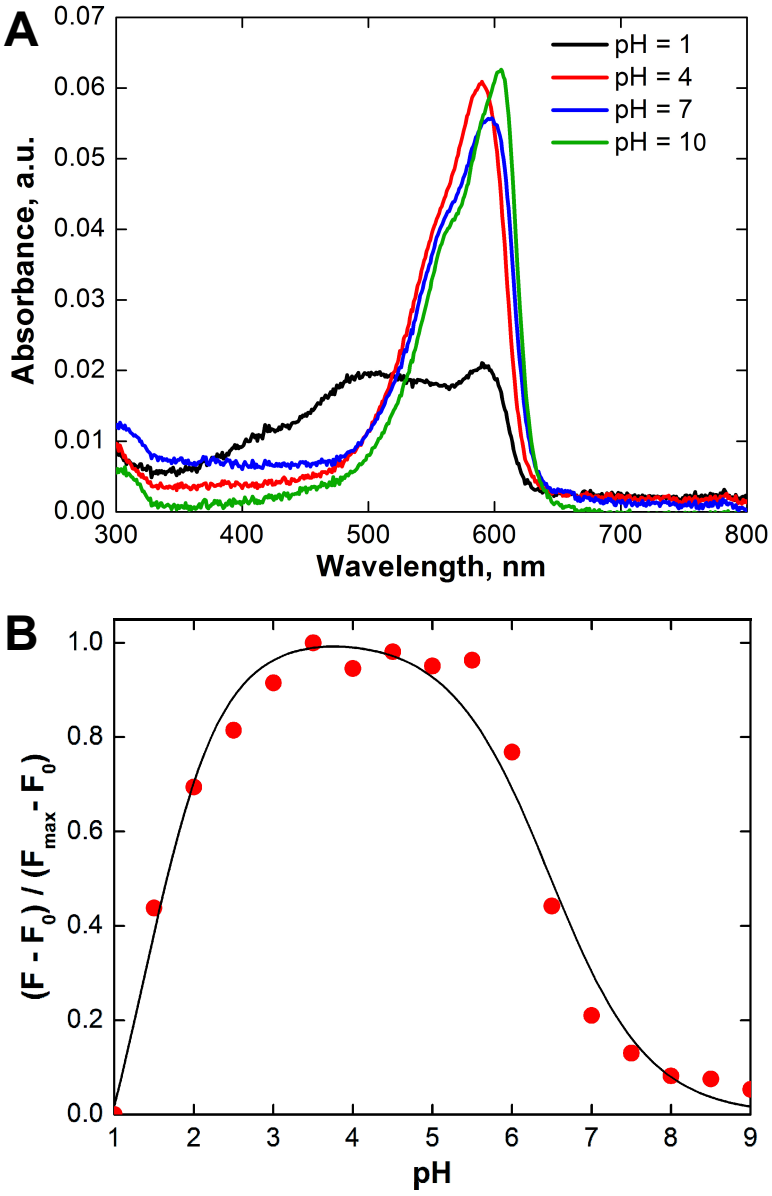

Figure S21. Effect of pH on an aqueous solution of ZR1. (A) Electronic absorption spectra recorded at various pH values. (B) Plot of the normalized integrated fluorescence emission vs pH, showing the nonlinear fit (continuous line) to the experimental data (red circles) used to determine the pK_a values (1 µM ZR1, 25 °C, 100 mM KCl, 20 mM AcONa, λ_{ex} = 560 nm). The two apparent pK_a values obtained for ZR1 were: pK_{a1} = 6.47 ± 0.1, pK_{a2} = 1.37 ± 0.18, R^2 = 0.9749.

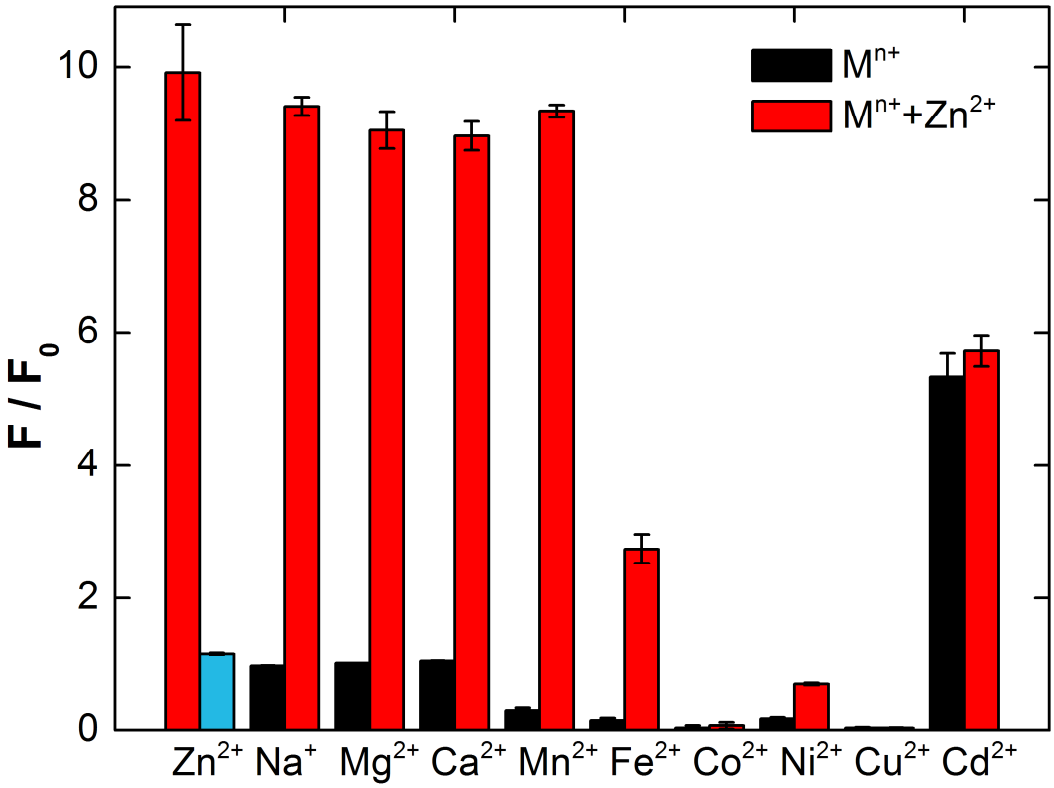

Figure S22. Metal selectivity of ZBR4 in aqueous buffer (25 °C, 100 mM KCl, 50 mM PIPES, pH 7.0, λ_{ex} = 560 nm). For each sample, the fluorescence emission was recorded before and 10 min after addition of excess (1 mM Na^{+}, Mg^{2+}, Ca^{2+}, 20 μM all other) metal ion of interest (black bars) to 1 μM ZBR4 and 1 μM EDTA. Subsequently, 20 μM $ZnSO_4$ (red bars) was added to each solution. The integrated fluorescence was normalized in each case to the fluorescence of the metal-free sensor. The blue bar indicates the average quenching of fluorescence emission upon addition of 250 μM EDTA to the Zn^{2+}-bound sensor solution.

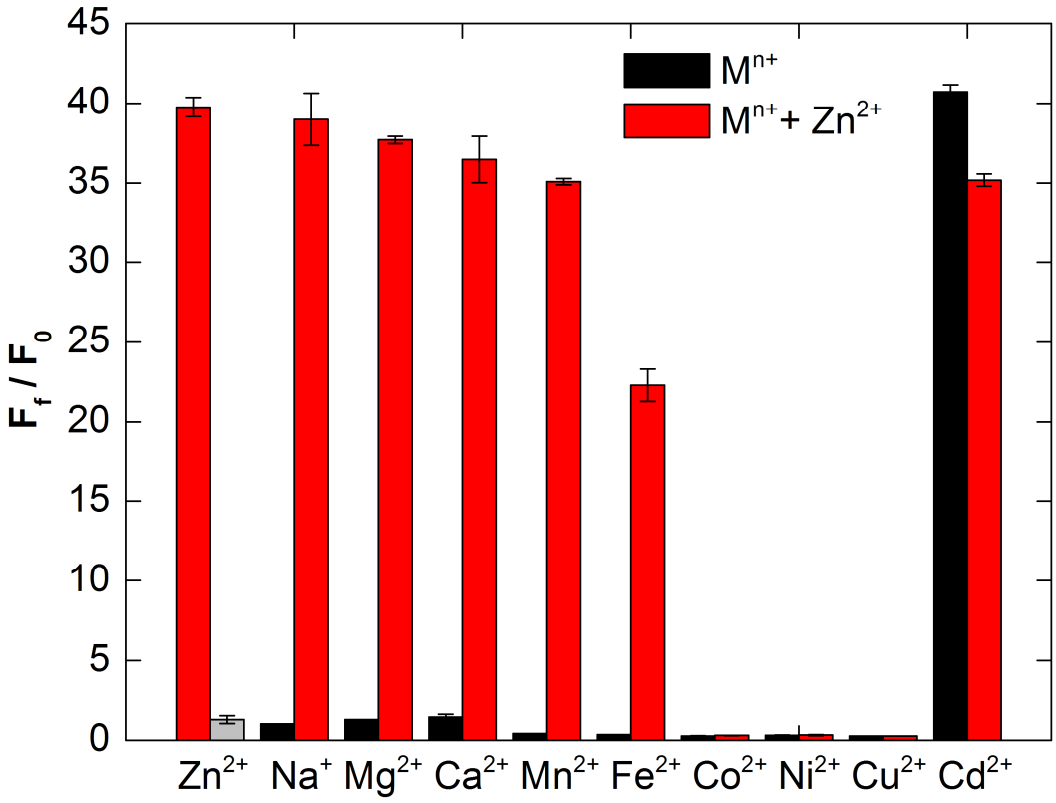

Figure S23. Metal selectivity of ZR1 in aqueous buffer (25 °C, 100 mM KCl, 50 mM PIPES, pH 7.0, λ_{ex} = 560 nm). For each sample, the fluorescence emission was recorded before and 10 min after addition of excess (2 mM Na^{+}, Mg^{2+}, Ca^{2+}, 50 μM all other) metal ion of interest (black bars) to 5 μM ZR1 and 5 μM EDTA. Subsequently, 50 μM $ZnCl_2$ (red bars) was added to each solution. The integrated fluorescence was normalized in each case to the fluorescence of the metal-free sensor. The gray bar indicates the average quenching of fluorescence emission upon addition of 250 μM EDTA to the Zn^{2+}-bound sensor solution.

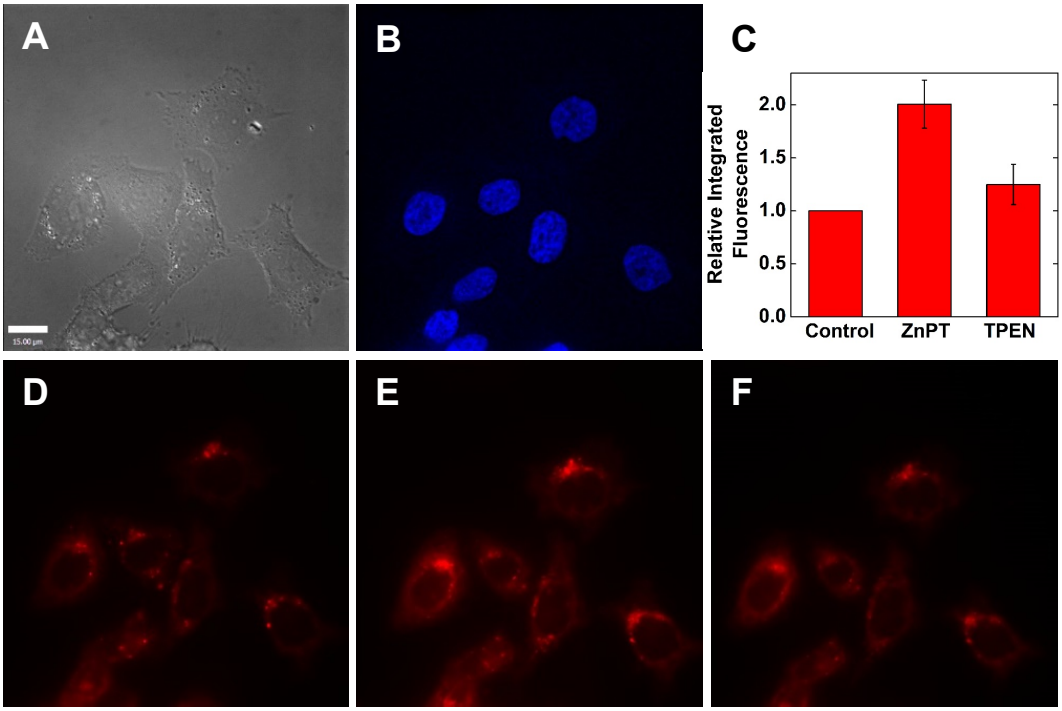

Figure S24. Fluorescence microscopy of live HeLa cells incubated with 2 μM ZR1 and 10 μM Hoechst 33258 at 37 °C for 15 min. (A) Differential interference contrast (DIC) image. (B) Nuclear staining by Hoechst 33258 (blue channel). (C) Quantification of Zn^{2+}-induced ZR1 fluorescence response (mean ± SD, N = 27). (D) ZR1 fluorescence without addition of exogenous Zn^{2+}. (E) ZR1 fluorescence 5 min after treatment with 50 μM Zn^{2+}/pyrithione = 1:2 (ZnPT). (F) ZR1 fluorescence 5 min after addition of 50 μM TPEN (red channel). Scale bar = 15 μm.

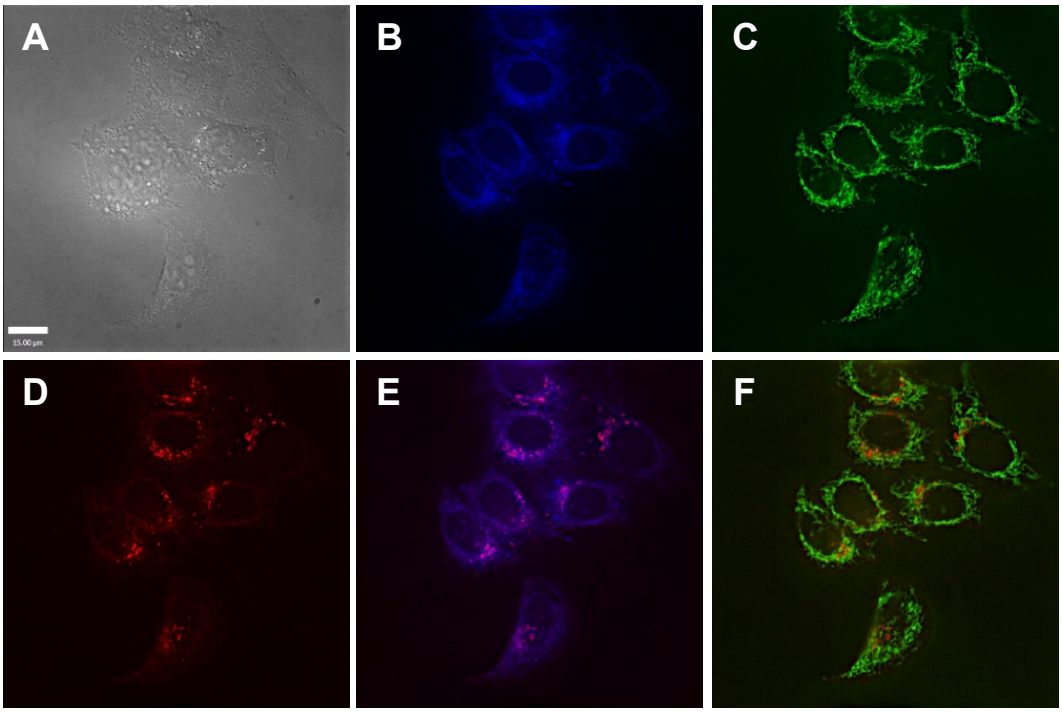

Figure S25. Co-localization analysis of ZR1 with organelle-specific markers in live HeLa cells incubated with 2 μM ZR1, 2 μM ER-Tracker Blue-White DPX, and 0.5 μM MitoTracker Green FM at 37 °C for 15 min. (A) DIC image. (B) ER-Tracker (blue channel). (C) MitoTracker Green (green channel). (D) ZR1 (red channel). (E) Overlay of ZR1 and ER-Tracker (Pearson's $r = 0.63 \pm 0.07$, $N = 50$). (F) Overlay of ZR1 and MitoTracker Green (Pearson's $r = 0.28 \pm 0.07$, $N = 40$). Scale bar = 15 μm.

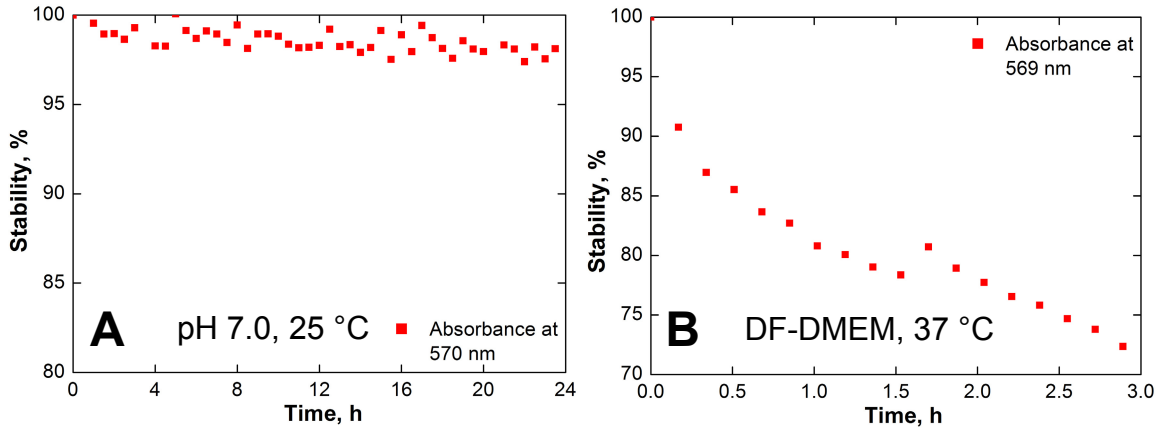

Figure S26. Stability of metal-free ZBR4 in aqueous solutions, judged by the relative absorbance values at the indicated absorption maxima. (A) 1.4 µM ZBR4, 25 °C, 100 mM KCl, 50 mM PIPES, pH 7.0. (B) 5 µM ZBR4, 37 °C, dye- and serum-free DMEM, pH 7.8.

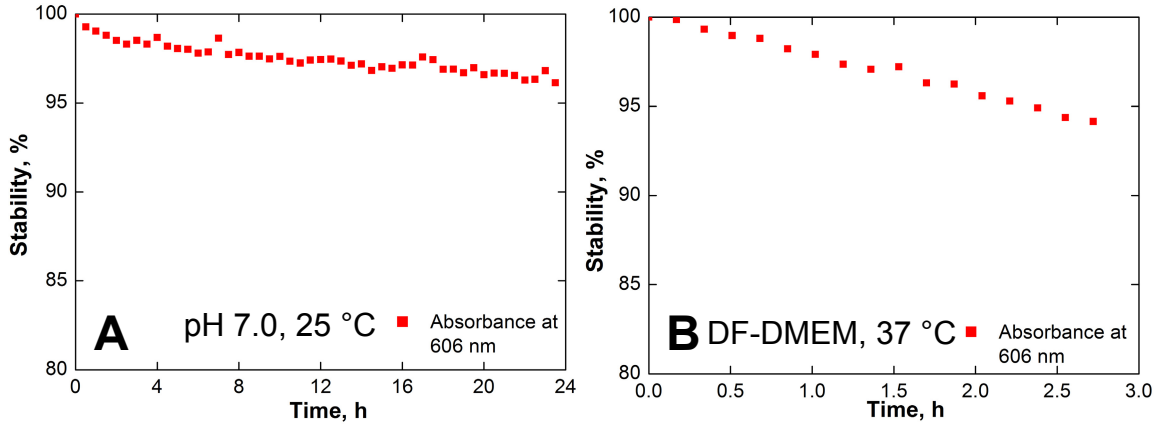

Figure S27. Stability of metal-free ZR1 in aqueous solutions, judged by the relative absorbance values at the indicated absorption maxima. (A) 5 µM ZR1, 25 °C, 100 mM KCl, 50 mM PIPES, pH 7.0. (B) 5 µM ZR1, 37 °C, dye- and serum-free DMEM, pH 7.8.

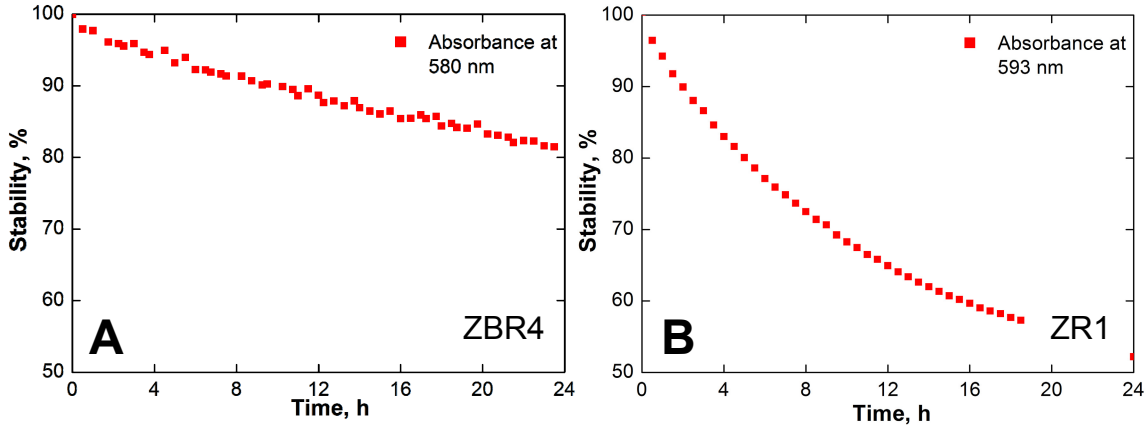

Figure S28. Stability of Zn^{2+}-bound ZBR4 and ZR1 in aqueous buffer, judged by the relative absorbance values at the indicated absorption maxima. (A) 1.4 µM ZBR4, 50 µM $ZnSO_4$, 25 °C, 100 mM KCl, 50 mM PIPES, pH 7.0. (B) 5 µM ZR1, 50 µM $ZnSO_4$, 25 °C, 100 mM KCl, 50 mM PIPES, pH 7.0.

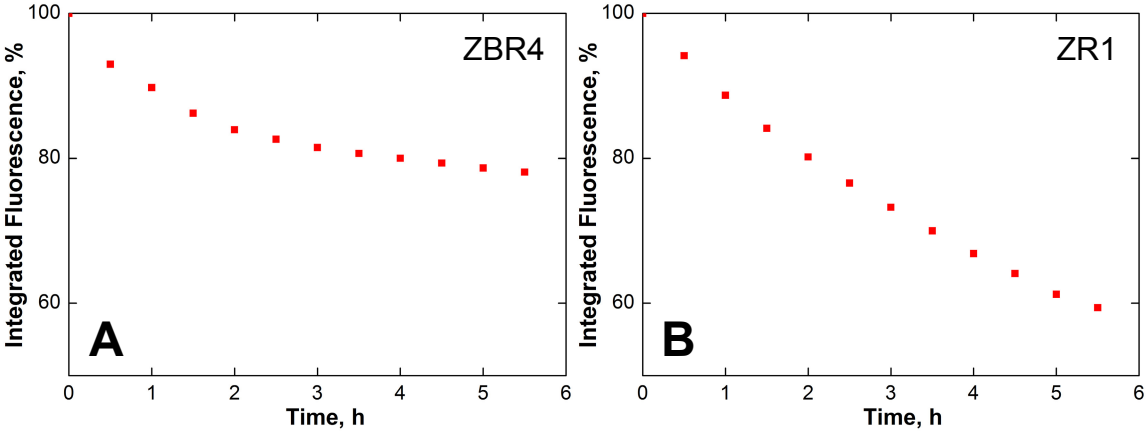

Figure S29. Relative integrated fluorescence emission over time of Zn^{2+}-bound ZBR4 and ZR1 in aqueous buffer (50 µM $ZnSO_4$, 25 °C, 100 mM KCl, 50 mM PIPES, pH 7.0). (A) 1 µM ZBR4. (B) 5 µM ZR1.

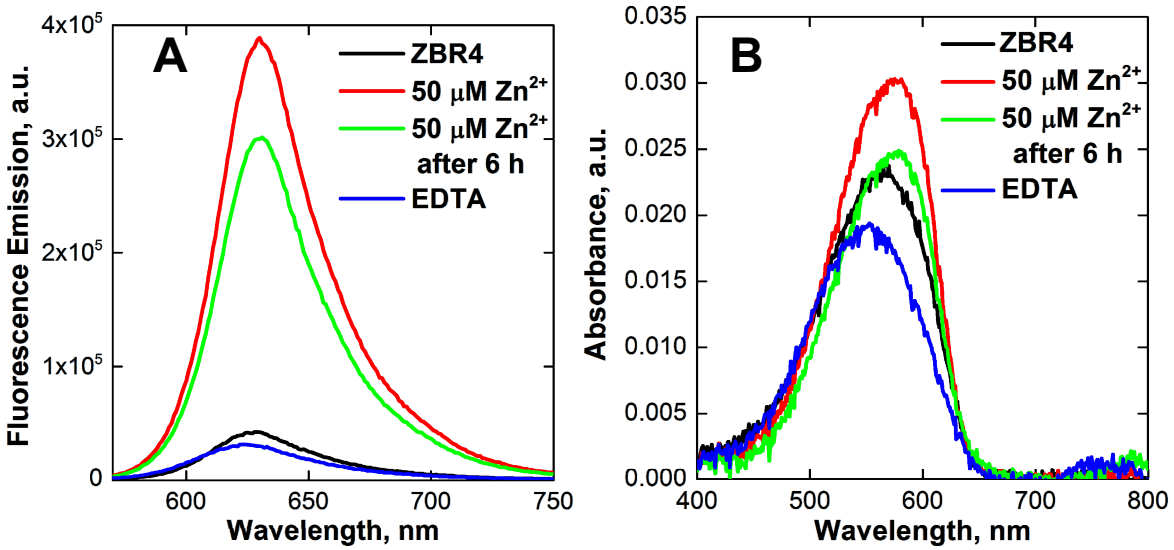

Figure S30. (A) Fluorescence emission and (B) electronic absorption spectra of a 1 μM solution of Zn^{2+}-bound ZBR4 in aqueous buffer, before and after addition of aq. EDTA at the 6 h mark in order to reverse the fluorescence turn-on (50 μM $ZnSO_4$, 250 μM EDTA, 25 °C, 100 mM KCl, 50 mM PIPES, pH 7.0).

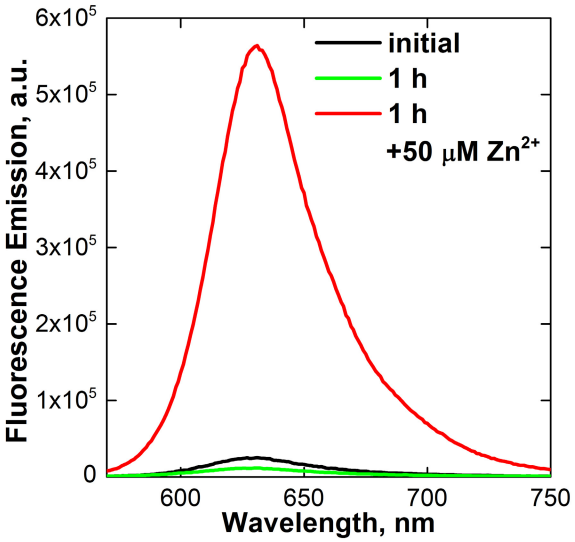

Figure S31. Fluorescence emission spectra of 5 μM ZBR4 in dye- and serum-free DMEM, taken at 37 °C before and after addition of 50 μM $ZnSO_4$ at the specified time points.

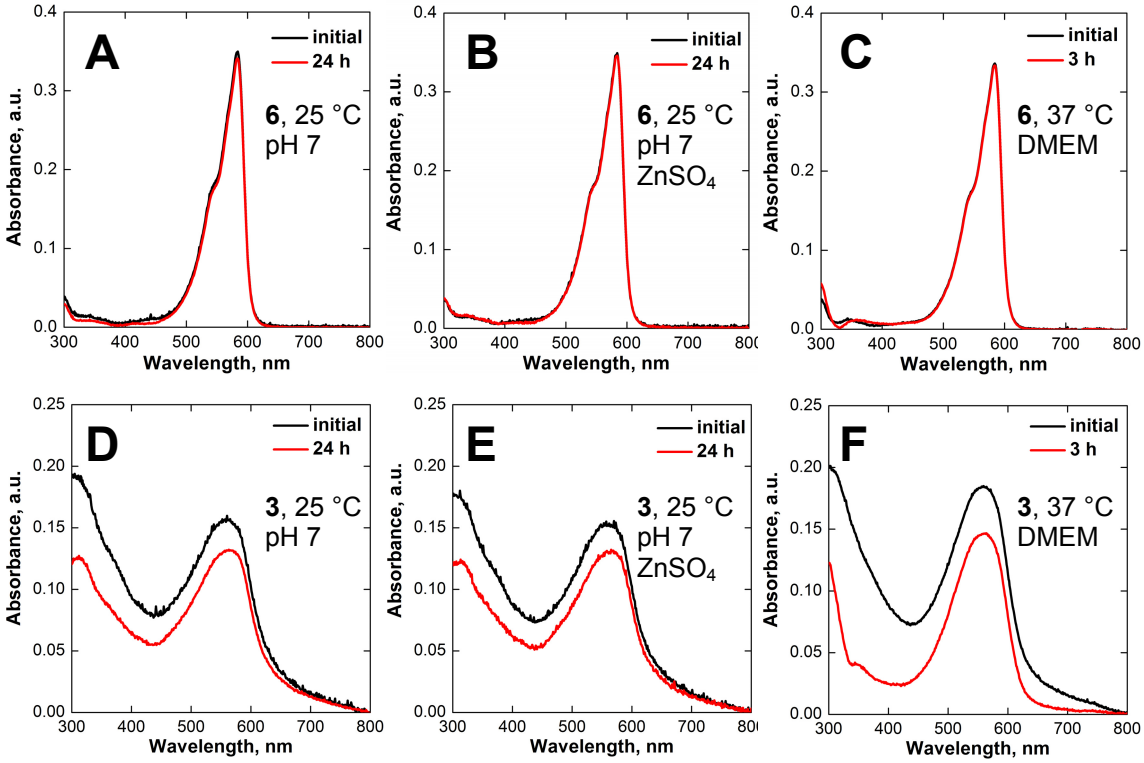

Figure S32. Stability of 5 μM solutions of (A-C) dichlororesorufin (**6**) and (D-F) chlorobenzoresorufin (**3**) in (A, B, D, E) aqueous buffer (25 °C, 100 mM KCl, 50 mM PIPES, pH 7.0) and (C, F) dye- and serum-free DMEM (37 °C, pH 7.8), monitored by absorption spectra taken at the specified time points. The solutions in (B) and (E) contained 50 μM of $ZnSO_4$. The decrease in the absorbance of **3** in (D), (E) and (F) is due to partial precipitation of the fluorophore in the cuvette during the acquisition period.

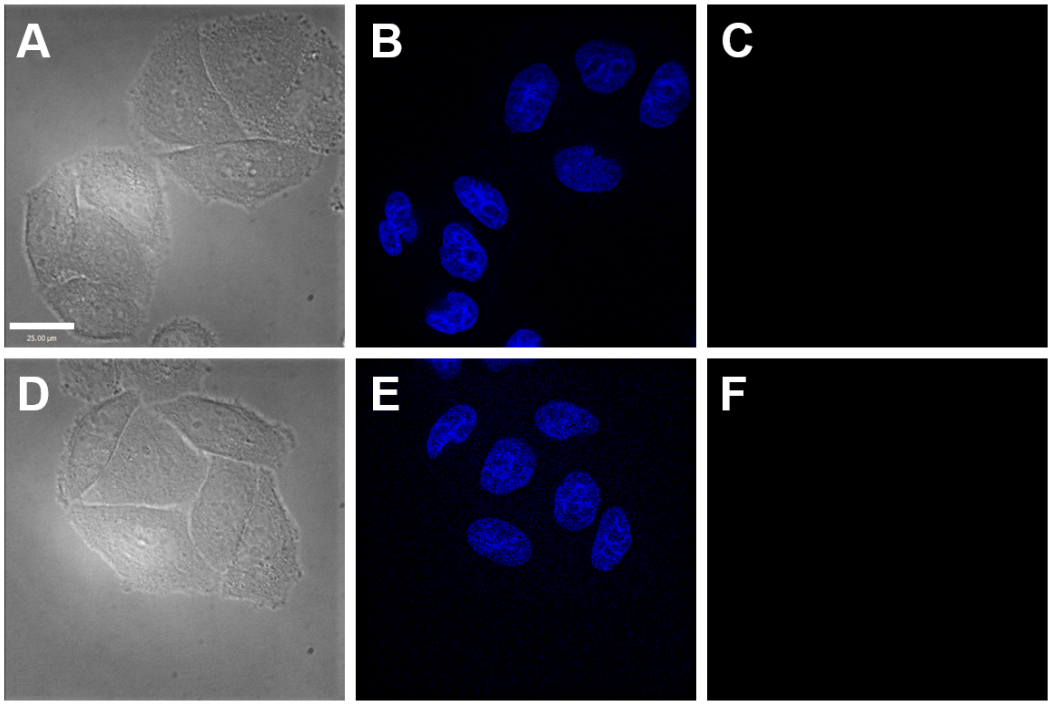

Figure S33. Fluorescence microscopy of live HeLa cells incubated with 15 μM Hoechst 33258, 5 μM chlorobenzoresorufin, **3** (top), and 5 μM dichlororesorufin, **6** (bottom), at 37 °C for 30 min, showing the cellular impermeability of the two fluorophores. (A,D) DIC images. (B,E) Nuclear staining by Hoechst 33258 (blue channel). (C,F) Fluorescence signal in the red channel. Scale bar = 25 μm.

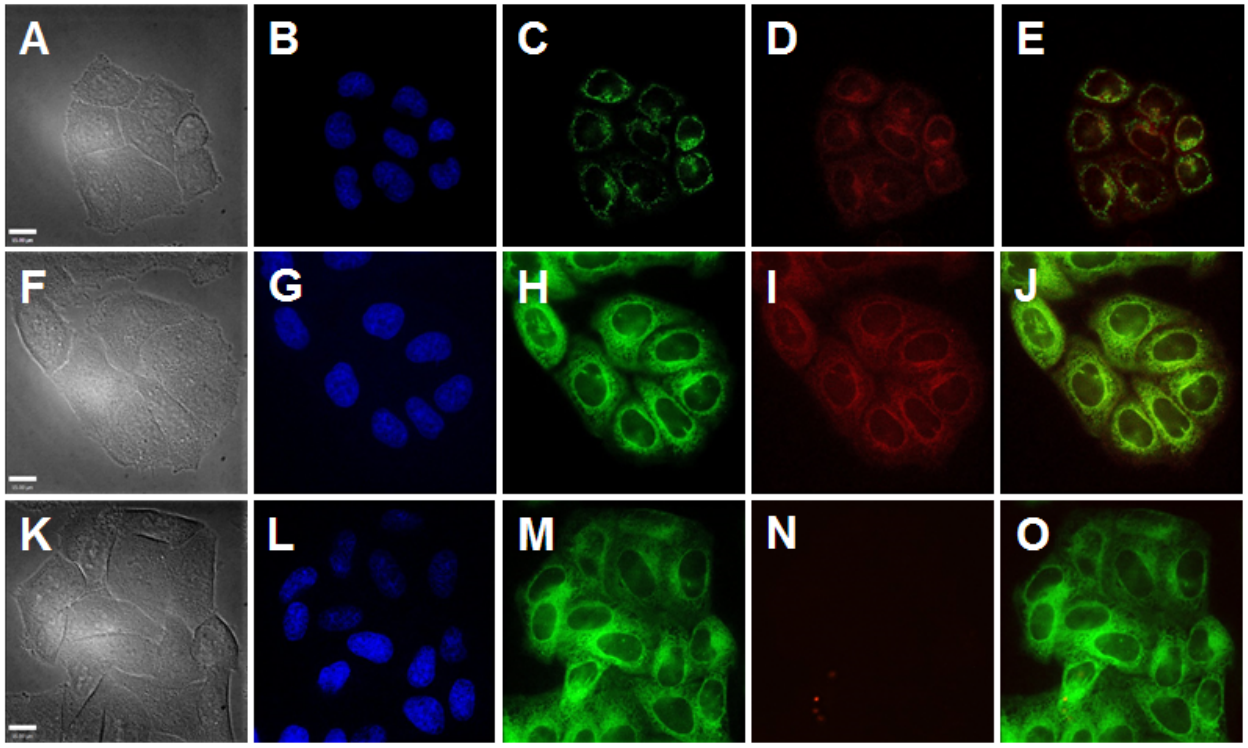

Figure S34. Fluorescence microscopy of live HeLa cells incubated with 15 µM Hoechst 33258, 0.5 µM MitoTracker Green (top), 0.5 µM ER-Tracker Green (middle, bottom), 5 µM chlorobenzoresorufin acetate, **4** (top, middle), and 5 µM dichlororesorufin acetate, **7** (bottom), at 37 °C for 30 min. (A,F,K) DIC images. (B,G,L) Nuclear staining by Hoechst 33258 (blue channel). (C) Nuclear staining by MitoTracker Green (green channel). (H,M) Nuclear staining by ER-Tracker Green (green channel). (D,I) Fluorescence signal of compound **4** (red channel). (N) Fluorescence signal of compound **7** (red channel). (E,J,O) Overlay of the green and red channels. Scale bar = 15 µm.

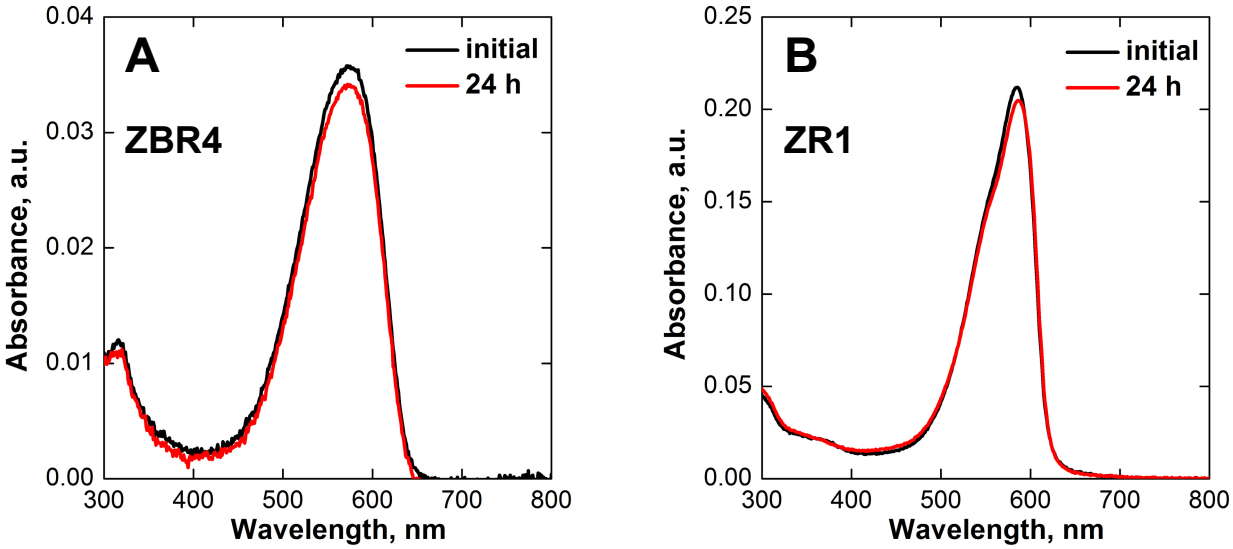

Figure S35. Stability of Zn^{2+}-saturated ZBR4 and ZR1 at 25 °C in deionized water with 100 mM KCl added. (A) 1.4 μM ZBR4, 50 μM $ZnSO_4$. (B) 5 μM ZR1, 50 μM $ZnSO_4$. Similar results (>95% stability) were obtained for the Zn^{2+}-saturated sensors in deionized water without KCl added, as well as for the metal-free forms in deionized water with or without 100 mM KCl added.

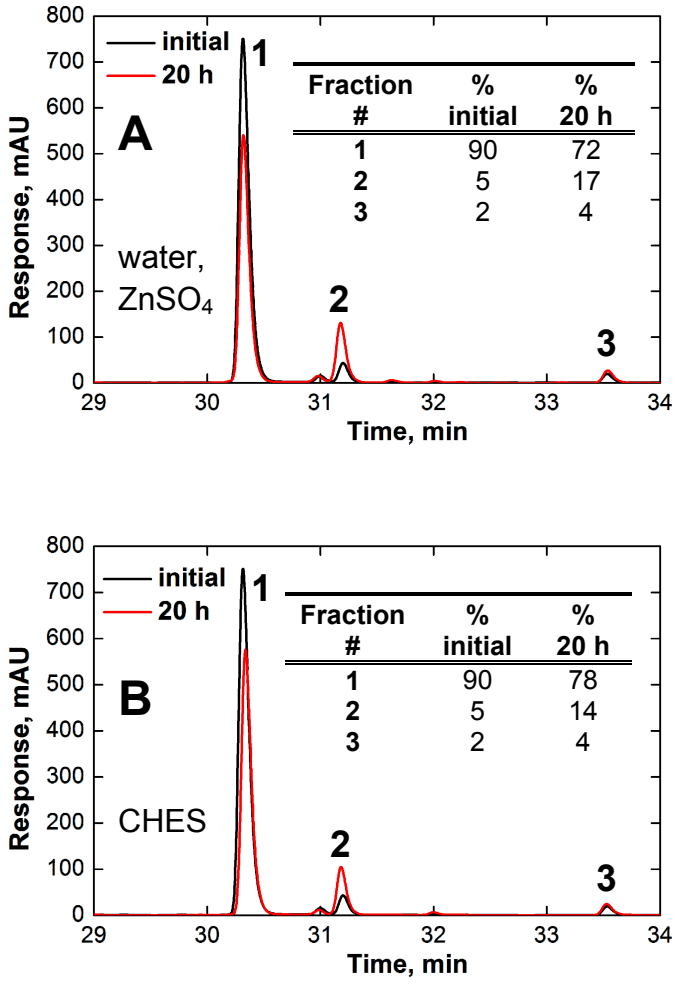

Fraction 1, ZR1

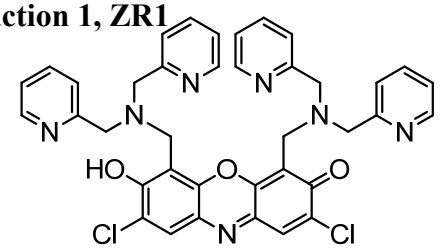

Calcd. for $[M+H]^+$ $C_{38}H_{32}Cl_2O_3N_7$: 704.2
Found: 704.2

Fraction 2

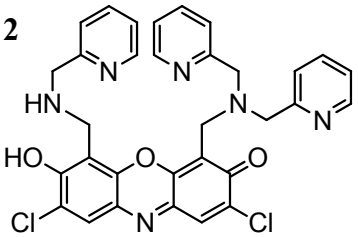

Calcd. for $[M+H]^+$ $C_{32}H_{27}Cl_2O_3N_6$: 613.2
Found: 613.2

Fraction 3

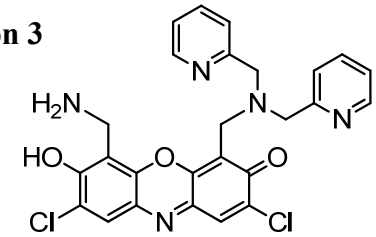

Calcd. for $[M-H]^-$ $C_{26}H_{20}Cl_2O_3N_5$: 520.1
Found: 520.7

Figure S36. Analytical HPLC and ESI-MS analysis of the degradation products of 45 µM aqueous solutions of ZR1, with the elution region of interest between 29 and 34 min expanded for clarity. (A) Deionized water, 90 µM $ZnSO_4$, 25 °C. (B) 10 mM CHES, pH 9.5, 25 °C. Low-resolution mass spectra of the isolated fractions were acquired in positive and negative mode. The chromatographic traces and composition of the product mixtures are based on the signal at 590 nm. No other products in significant amounts (>1%) were detected by the signals at 220, 280 and 500 nm (not shown).

References

(1) Gottlieb, H. E.; Kotlyar, V.; Nudelman, A. *J. Org. Chem.* **1997**, *62*, 7512-7515.

(2) Bueno, C.; Villegas, M. L.; Bertolotti, S. G.; Previtali, C. M.; Neumann, M. G.; Encinas, M. V. *Photochem. Photobiol.* **2002**, *76*, 385-390.

(3) French, A. P.; Mills, S.; Swarup, R.; Bennett, M. J.; Pridmore, T. P. *Nat. Protoc.* **2008**, *3*, 619-628.

(4) Burdette, S. C.; Walkup, G. K.; Spingler, B.; Tsien, R. Y.; Lippard, S. J. *J. Am. Chem. Soc.* **2001**, *123*, 7831-7841.

(5) Walkup, G. K.; Burdette, S. C.; Lippard, S. J.; Tsien, R. Y. *J. Am. Chem. Soc.* **2000**, *122*, 5644-5645.